JOURNAL OF GEOPHYSICAL RESEARCH, VOL. 93, NO. B11, PAGES 13,332-13,354, NOVEMBER 10, 1988

ACTIVE DEFORMATION IN THE NEW GUINEA FOLD-AND-THRUST BELT: SEISMOLOGICAL EVIDENCE FOR STRIKE-SLIP FAULTING AND BASEMENT-INVOLVED THRUSTING

Geoffrey Abers and Robert McCaffrey[1]

Department of Earth, Atmospheric, and Planetary Sciences
Massachusetts Institute of Technology, Cambridge

Abstract. The New Guinea fold-and-thrust belt forms a 1000-km-long mountain chain running the length of New Guinea, but its trend is oblique to the predicted convergence direction. A large component of left-lateral shear across the mountain belt is expected, but geological evidence for such motion is ambiguous. Surface structures in the fold-and-thrust belt show mountain building by folding and thrusting, supposedly thin skinned, of pre-Pliocene continental shelf sediments, although some evidence indicates that active faulting penetrates the basement. We examine the active deformation of this mountain belt by using teleseismic long-period P and SH waveforms, short-period P waveforms, and P wave first motions to determine reliable focal mechanisms and source depths for the 18 largest earthquakes in the New Guinea fold-and-thrust belt since 1964. Eight thrust events, with seismic moments (M_0) between 10^{17} and 2 x 10^{18} N m, are distributed throughout the thrust belt at depths ranging from 0.5 to 45 km and have steeply dipping fault planes that strike parallel to surface structural trends. Six of the eight events are between 11 and 25 km deep. The steep dips of nodal planes, the depths of these earthquakes, and the known thicknesses of the sedimentary section show that thrust faulting is not exclusively thin skinned (i.e., confined above a shallow detachment surface) but penetrates the crystalline basement at high angles. Most earthquakes in the western half of the thrust belt, including the three largest earthquakes examined (M_0 > 5 x 10^{18} N m), show strike-slip faulting with the probable fault plane oriented east-west, so that displacement is left lateral. The nine strike-slip earthquakes account for almost 90% of the observed seismic moment in the period 1964-1985 and indicate a seismic slip rate of 5-25 mm/a. All but one of these strike-slip earthquakes are shallower than the thrust earthquakes, suggesting that east-northeast convergence across the fold-and-thrust belt is accommodated by a decoupled system of strike-slip and dip-slip faults. While the great height of the mountain belt is an obvious indication that crustal thickening is an important consequence of plate motion in New Guinea, seismological evidence suggests that translation by strike-slip faulting may play a much greater role than previously recognized. By analogy, in older collisional orogens, whose motions can be inferred only from remnant structures and not from seismicity, strike-slip faulting may have been equally important in accommodating convergence. We estimate from seismic moments of earthquakes and from the volume of the mountains that deformation of the New Guinea Highlands may account for 5-20% of the total convergence between the Pacific plate and Australia in New Guinea.

Introduction

Central New Guinea is one of the few places where an arc-continent collision is actively producing a mountain belt, and as such serves as a type area for present-day continental accretion [e.g., Dewey and Bird, 1970], yet little is known about active processes there. New Guinea was the passive northern margin of the Australian continent throughout Mesozoic and early Cenozoic time, until one or more volcanic arcs collided with it in the late Cenozoic [e.g., Hamilton, 1979]. Present-day deformation is a consequence of continued convergence between the Pacific and Australian plates and is unevenly distributed over the northern 200 km of the island, with most activity in the mountains or near the north coast. Seismic activity near the north coast (Figure 2) accounts for some of the convergence across the island and will be discussed in a later paper. Because plate convergence is highly oblique to the trend of the island (Figure 1), deformation in New Guinea is not purely compressional but must include a large component of left-lateral shear. The growth of the mountains in New Guinea therefore provides an active example for continental accretion and oblique convergence in older mountain belts such as the North American Rockies [e.g., Silver and Smith, 1983].

We examine the active tectonics of the fold-and-thrust belt, which produces most of the mountainous topography in New Guinea. The mountains, referred to as the Highlands, form the central spine of New Guinea from 135°E to 145°E, with peaks 3 to 5 km above the adjacent foreland basin. We use teleseismic body waveforms to constrain depths, mechanisms, and seismic moments of the largest earthquakes there. One concern is whether or not detachment faulting is the sole mode of shortening in the fold-and-thrust belt. Depths of earthquakes reported in catalogs of seismicity provide little or misleading information because depths of shallow earthquakes can be in error by many tens of kilometers [e.g., Jackson, 1980], even when "pP" is used [McCaffrey, 1988]. By analyzing teleseismic waveforms we are able to determine depths of thrust earthquakes to within 2-5 km and of

[1]Now at Department of Geology, Rensselaer Polytechnic Institute, Troy, New York.

Paper number 7B5097.
0148-0227/88/007B-5097$05.00

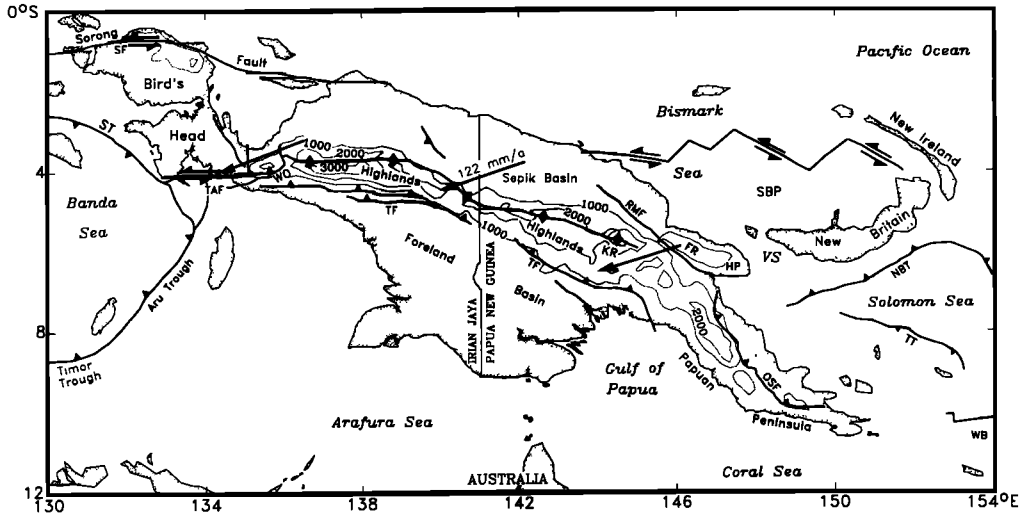

Fig. 1. Map of New Guinea showing regional structures, tectonic provinces, geographical names, topography, and direction of Pacific-Australia plate convergence. Structures from Hamilton [1979], Dow et al. [1986], and Doutch [1981]. Pacific-Australia plate-convergence vectors are shown as arrows, with arrowheads at the location the vectors were calculated and arrow length proportional to velocity (labelled for arrow at 140°E), from instantaneous plate motion poles of Minster and Jordan [1978]. Topography is contoured every 1000 m above sea level (dotted lines) and is labeled in meters [Heirtzler, 1985]. Abbreviations: FR, Finisterre Range; HP, Huon Peninsula; KR, Kubor Range; OSF, Owen Stanley Fault; NBT, New Britain Trench; RMF, Ramu-Markham Fault; SBP, South Bismark Plate; SF, Sorong Fault; ST, Seram Trough; TAF, Tarera-Aiduna Fault; TF, Thrust Front; TT, Trobriand Trough; VS, Vitiaz Strait; WB, Woodlark Basin; WO, Weyland Overthrust. The Medial Suture zone is indicated by solid diamonds, thrust faults are indicated by solid triangles on the presumed hanging wall, and strike-slip faults are indicated by split arrows.

strike-slip earthquakes to within 7-10 km, allowing us to distinguish between thin-skinned and basement-involved faulting. The second objective of this study is to investigate how oblique convergence affects mountain building in the thrust belt. By constraining the focal mechanisms and seismic moments we establish the relative importance of crustal thickening and left-lateral shear in the mountains. We estimate the spatial extent of strike-slip faulting within the mountains and its relationship to thrust faulting. Our results show that there is high-angle thrust faulting within the basement beneath assumed detachment faults and that most earthquakes result from left-lateral strike-slip faulting parallel to the mountain front.

Tectonic setting

Regional Geology. Large-scale structures on New Guinea trend roughly WNW-ESE (Figure 1) and can be grouped into four provinces from south to north [Dow, 1977]: the stable platform/foreland basin, the fold-and-thrust belt, the mobile belt, and a belt of former island arcs. These divisions are relevant only to central New Guinea, and do not describe structures in the Papuan peninsula in the east or the Bird's Head in the west. Most geologic observations are from Papua New Guinea (PNG) and the western third of Indonesian New Guinea (Irian Jaya); little surface mapping has been done in the main part of Irian Jaya [Dow and Sukamto, 1984b].

The stable Australian platform is covered by a Mesozoic and Cenozoic sedimentary sequence. Most sediments older than early to mid Miocene were deposited in a passive margin setting, while present-day deposits on the platform and foreland basin are dominated by clastic sediments derived from the Highlands [e.g., Davies, 1978; Dow, 1977]. North of the foreland basin a sequence of folded and faulted platform rocks makes up a fold-and-thrust belt that extends through much of the Highlands. Paleozoic basement rocks similar to those on the Australian mainland have been found beneath the platform sequence, at least as far north as the Kubor Range in the east [Bain et al., 1975] and at scattered localities in the western mountains [e.g., Dow and Sukamto, 1984b; Visser and Hermes, 1962]. The mobile belt assemblage north of the suture includes deep-water sediments, volcanic rocks, and ultramafic intrusives that are intensely deformed and have undergone metamorphism up to blueschist grade [e.g., Hamilton, 1979]. Ophiolites have been identified throughout the mobile belt on the northern flanks of the Highlands [e.g. Davies, 1982; Dow and Sukamto, 1984a, b], providing evidence for the closing of an ocean basin. Rocks along the north coast reveal former island arcs active until Miocene times [e.g., Dow, 1977]. Mountains along the north coast are separated from the Highlands by a series of Neogene basins.

Fold-and-thrust belt. The fold-and-thrust belt, the focus of this paper, extends from the medial suture to the southern limit of deformation and incorporates Cenozoic and some Mesozoic shelf sediments in south verging

asymmetric folds and north dipping thrust faults [Dow, 1977; Jenkins, 1974]. Competent Tertiary carbonate sequences form imbricate thrust sequences in eastern parts of the thrust belt, suggesting that surface faults are confined above a décollement [Findlay, 1974; Hobson, 1986; Jenkins, 1974]. In the western thrust belt, shales are predominant and rarely form coherent thrust sheets [Hamilton, 1979], and faulting includes Paleozoic rocks in places [Dow and Sukamto, 1984b]. The deformation front is advancing south over the foreland basin and is currently incorporating sediments younger than 0.2 Ma; Pliocene molasse originally deposited at the axis of the Pliocene basin is now involved in folding [Hamilton, 1979]. Erosional patterns in Irian Jaya show Quaternary uplift of the southern foothills concurrent with subsidence of the adjacent foreland basin [Visser and Hermes, 1962], also suggesting that the frontal thrusts are still advancing southward.

Mapping in the region south of the Kubor Range shows that older rocks are not included in thrust sheets, and a few drill holes show that the oldest rocks are undisturbed, suggesting that décollements in the fold-and-thrust belt are located in the Mesozoic or early Cenozoic sedimentary layers [e.g., Dow, 1977; Dow and Sukamto, 1984a; Findlay, 1974; Hamilton, 1979; Hobson, 1986; Jenkins, 1974] and that deformation is confined to the upper 5-10 km of the crust. Mapping in other parts of the thrust belt, however, suggests that faulting extends into the basement [e.g., Davies, 1978, 1982]. Uplifted sections of basement rocks, such as the Kubor uplift [Bain et al., 1975], are found in parts of the thrust belt. Reported depths of earthquakes have been used as evidence that some faulting penetrates the crystalline basement [Ripper and McCue, 1983].

Distribution of left-lateral shear. Solutions for global plate motions [Minster and Jordan, 1978] predict ~120 mm/a convergence between the Pacific plate and Australia at an azimuth of 70° across New Guinea (Figure 1), but the north coast, the major faults, and the trends of the deforming zones are far from perpendicular to this azimuth. The predicted convergence direction suggests either that faulting is oblique or that deformation is segregated into left-lateral strike-slip faulting and pure dip-slip faulting (analogous to faulting in Sumatra, Japan, and the Philippines [Fitch, 1972]).

In eastern New Guinea much of the left-lateral component of Pacific-Australia motion may occur offshore. The eastern quarter of New Guinea is south of the "South Bismark" plate (Figure 1), which moves ESE with respect to the North Bismark Sea at 90-100 mm/a [Taylor, 1979]. The resulting motion between the south Bismark plate and Australia is almost perpendicular to the trend of structures in New Guinea at a rate of ~50 mm/a, and is consistent with predominantly thrust mechanisms for fault plane solutions in eastern New Guinea [e.g., Cooper and Taylor, 1987; Johnson and Molnar, 1972; Weissel et al., 1982; G. Abers, unpublished results].

The ~100 mm/a of left-lateral motion is harder to account for in central and western New Guinea where no offshore transform-fault systems are observed. In the northern Bird's Head region there is geological evidence for ~400 km of left-lateral slip on the Sorong fault zone since late Miocene [Dow and Sukamto, 1984a], and large strike-slip earthquakes show that it is still active [Giardini et al., 1985]. Seismicity north of the mountains in the central part of the island is associated with the coastal mountains and the Neogene basins. Published focal mechanisms (Cooper and Taylor [1987]; centroid-moment tensor solutions) and our preliminary waveform solutions for these events largely show thrust faulting.

The Tarera-Aiduna fault zone in the south displays features of a strike-slip fault [Dow and Sukamto, 1984a; Hamilton, 1979], although there are no geological constraints on the sense or amount of slip [Pigram and Panggabean, 1983]. The surface expression of the Tarera-Aiduna fault zone apparently ends at the Weyland Overthrust [Dow and Sukamto, 1984a], and the only mapped strike-slip faults east of 136°E are tear faults, striking at high angles to the thrust belt [Pigram and Panggabean, 1983]. In Eastern Irian Jaya, where surface geological mapping is sparse, only thrust faults have been mapped south of the suture zone [Dow and Sukamto, 1984a; Dow et al., 1986].

Waveform Inversion

Focal mechanisms and depths were determined for large earthquakes in the fold-and-thrust belt (Figures 2 and 3; Table 1) using least squares inversion to match teleseismic body waves. Eighteen earthquakes with useable body waves occurred south of the medial suture since 1964. Long-period and short-period P waveforms and long-period SH waveforms were digitized from analog records of the World-Wide Standard Seismograph Network (WWSSN) or taken from Global Digital Seismograph Network (GDSN) digital tapes. Analog records were interpolated at 0.5- and 0.1-s intervals for long- and short-period data, respectively, and long-period GDSN seismograms were sampled at 1 s. Linear trends were removed from the seismograms, and the waveforms were windowed to include the first 1 to 2 min of the P and SH phases. P and SH wave records were limited to epicentral distance ranges of 30° to 90° and 30° to 75°, respectively, in order to avoid complications in the observed signal caused by propagation in the upper mantle or near the core-mantle boundary. Because the amplitudes of short-period seismograms differed by factors of 2 or more between nearby stations, they were normalized to the RMS amplitude for each seismogram [McCaffrey and Nábělek, 1984] and were not used in the estimates of seismic moment.

The waveform inversion method [McCaffrey and Abers, 1988] is similar to that of Nábělek [1984, 1985] and is based on the method for calculating far-field displacement due to a point dislocation source developed by Langston and Helmberger [1975]. Waveforms are treated as a combination of direct phases (P or SH) and phases reflected from the earth's surface (pP, sP, or sS), modified by a receiver instrument response, geometrical spreading, and mantle attenuation, described by a t^* [Futterman, 1962] of 1 s for compressional waves and 4 s for shear waves (errors in t^* affect estimates of moment and source duration but have little effect on other parameters [Nábělek, 1984]). Analysis of

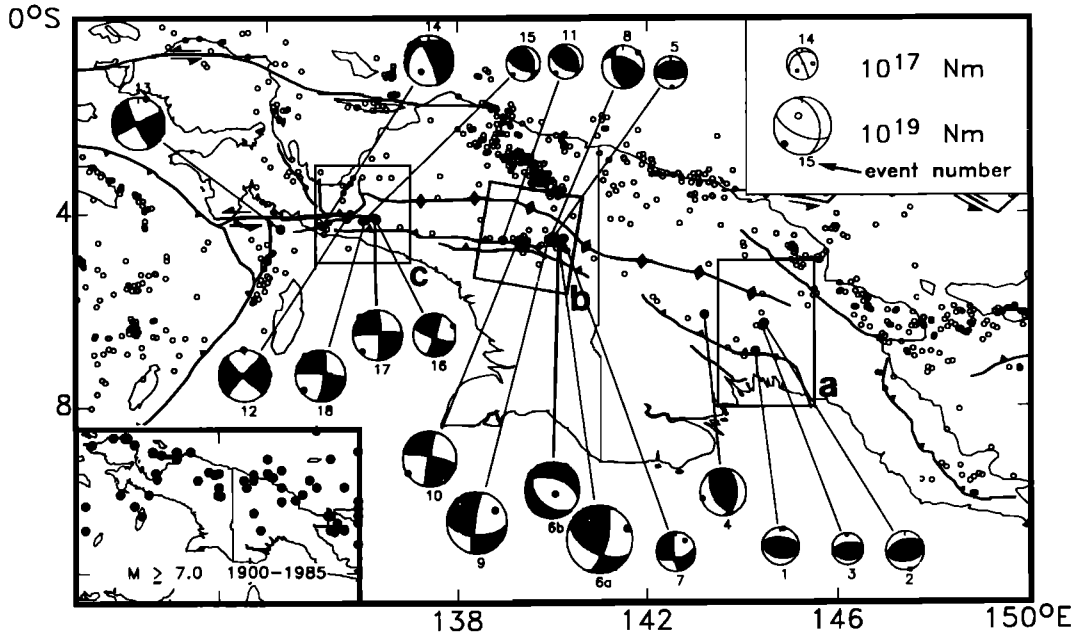

Fig. 2. Map of focal mechanisms determined here, locations of cross sections in Figure 11, and shallow seismicity. Focal mechanisms are shown as lower hemisphere projections with the compressional quadrants shaded, and the P and T axes shown as solid and open circles, respectively. The sizes of the focal spheres are scaled to log (M_0), according to the scale in the upper right, and are labeled by the event numbers in Table 1. Seismicity is from the ISC catalog, 1964-1984, and includes all events listed as being shallower than 70 km recorded by 25 or more stations, with $M_b \geq 5.0$, and with standard deviations in latitude, longitude, or depth each not exceeding 20 km. Inset in lower left shows all large ($M \geq 7.0$), shallow ($\leq$ 70 km) earthquakes in the period 1900-1985, from the catalog compiled by Everingham [1974] for events before 1971 and from Ganse and Nelson [1981, with supplement] for more recent events. Faults are labelled on Figure 1.

smaller events from Irian Jaya with simple source time functions shows that source structure there is sufficiently represented by a homogeneous half-space with assumed compressional velocity (V_p) of 6.5 km/s, shear velocity (V_s) of 3.7-3.9 km/s, and density (ρ) of 2800 kg/m^3. One layer representing sediments (V_p = 4.5 km/s, V_s = 2.7 km/s, and ρ = 2400 kg/m^3) over a crustal half-space was used to describe structure in PNG, to facilitate comparison with geological cross sections [Hobson, 1986]. For event 11, at 45 km depth, we described the source structure with a 38-km crustal layer overlying a mantle half-space (assumed that V_p = 8.0 km/s, V_s = 4.5 km/s, and ρ = 3300 kg/m^3). The source-time function is parameterized by a series of triangular elements whose amplitudes are determined in the inversion [e.g., Nábělek, 1984, 1985] but are required to be positive. The double-couple source is described by the strike and dip of one nodal plane, the slip direction on that plane, using the convention of Aki and Richards [1980], the depth, the seismic moment, and the source-time function shape.

Source parameters were determined by a least squares minimization of amplitude residuals between the observed and calculated seismograms (Table 2). In order to reduce the number of degrees of freedom in the inversions, initial solutions were constrained to have simple source-time functions. A longer and more finely sampled source time function was allowed when the mechanism had converged to stable values. Mechanisms based on P wave first motions picked from WWSSN records were used as starting models, and starting arrival times were estimated from the ISC hypocenters and the Jeffreys-Bullen travel time tables. In one case (event 11), short-period first motions are used to constrain the final solution. Once the solution had converged, the starting times for the observed seismograms were adjusted by maximizing the cross correlation between the calculated and observed waveforms, but arrival times were constrained to match clear first arrivals, if present, to within 1.0 s. Cross correlation without constraining the arrival times of the direct phases can lead to a depth bias if the amplitudes of reflected phases are much larger than the direct arrival. Arrival times for some emergent long-period waveforms were picked from corresponding short-period records.

In the appendix we analyze uncertainties in the waveform inversion procedure. For events with long-period data only, uncertainties in depth are typically less than 5 km for high-angle thrust earthquakes and 5-10 km for strike-slip earthquakes, and a few events with short-period data have smaller uncertainties in depth. The strike of nodal planes can be constrained to within 10° for the strike-slip earthquake mechanisms and within 10°-20° for high-angle

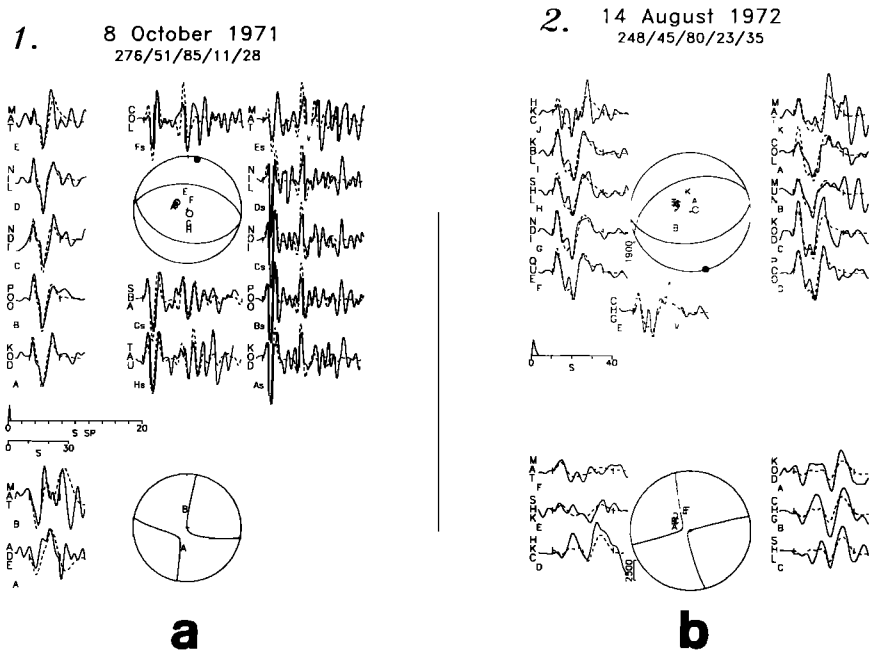

Fig. 3. Waveforms and solutions for all events studied. The events are labelled in the upper left by the number in Table 1 and by date at the top. Below the date is the mechanism, in the format strike(°)/ dip(°)/ rake(°)/ depth(km)/ moment(x10^{16} N m). P waves are shown on top, and SH waves are on the bottom, with the nodes of the corresponding radiation patterns in the focal spheres. Small solid and open circles on the P wave focal sphere designate the P and T axes, respectively. Solid lines are observed seismograms, dashed lines are calculated. The source-time function and time scale are shown on the left, between P and SH waves. Seismogram amplitudes are corrected to a magnification of 3000 and a distance of 40°, and the scale in microns is at the lower left of the focal spheres. Small letters in the focal spheres show positions of rays to stations and correspond to letters next to the waveforms below the station names. A small "s" and a small "d" next to letter by the seismogram indicates short-period and digital seismograms, respectively. Short-period data are shown with a separate time scale, labelled "S SP". For event 1 each seismogram amplitude is normalized by its root-mean-squared amplitude, rather than source amplitude. Event 6 shows a double event, with the second subevent indicated by dotted nodal planes and source-time function. Event 11 shows first-motion polarities used to constrain the mechanism, with open circles representing dilatational arrivals, plus signs representing compressional arrivals, dots representing nodal arrivals, and smaller symbols representing emergent arrivals.

thrust mechanisms depending on the distribution and quality of SH waveforms. The inversion results are insensitive to the number of stations used as long as the stations are well distributed in azimuth. A poor distribution, however, can bias the inversion results; we found that waveforms from stations in Asia can indicate depths 5-6 km greater than waveforms from Australian stations. The smallest earthquakes studied were recorded only by high-gain stations in Asia, and consequently their source parameters are less well constrained.

Results

Earthquakes in the Papua New Guinea Fold-and-Thrust Belt

October 8, 1971 (Event 1). Of the events studied, the 1971 earthquake is the closest to the southern thrust front in Papua New Guinea (Figures 2 and 4), where faulting is often assumed to be confined above a low-angle detachment thrust [e.g., Dow, 1977; Hamilton, 1979]. A thrust mechanism was found similar to that of Ripper and McCue [1983], with steeply dipping nodal planes striking parallel to thrusts and folds near the epicenter (Figures 2 and 3a). The calculated depth for the earthquake is 11 ± 3 km, placing it in either the uppermost basement or the lowermost part of the Triassic-Jurassic sequence [Hobson, 1986] but well below the suspected detachment. We examined the earthquake depth in detail (Figure 5) to verify that the depth of the earthquake is considerably deeper than the 5 km depth for the detachment horizon determined by Hobson [1986].

The velocity structure assumed for events 1-4, a 9-km-thick upper layer representing sediments over a crustal half-space, simulates a balanced cross section located 5-10 km along strike from events 1-3 [Hobson, 1986, cross-section 4]. Hobson shows a sediment-basement interface, interpreted from seismic profiles, lying 10 km below the surface near the thrust front and dipping gently to the north. The same structure

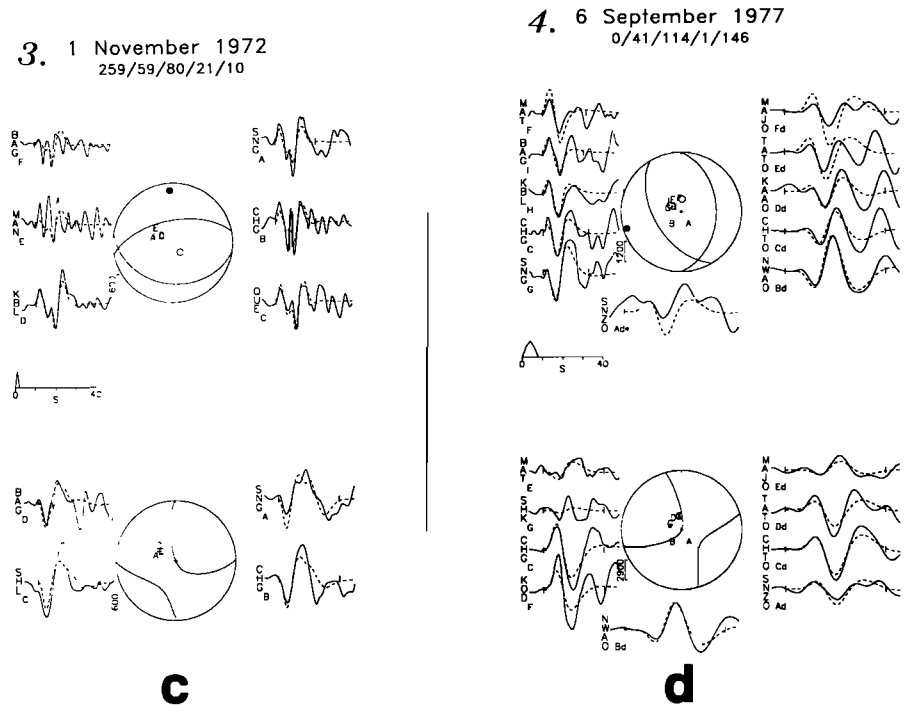

Fig. 3. (continued)

is assumed for all four events in PNG to simplify comparison of their depths.

The source duration for the earthquake was short (Table 2), so distinct phases are visible in short-period seismograms. Arrivals were identified in the short-period seismograms 4.5-5.0 s after the direct P arrival and have the correct polarity for pP from the free surface

TABLE 1. Earthquake Locations and Previous Solutions

Event	Date	Time	Latitude °S	Longitude °E	M_b	M_s[a]	Nsta[b]	Previous Solutions[c]
			Papua New Guinea					
1	Oct. 8, 1971	1415:36.5	6.87	144.27	5.6		127	RM
2	Aug. 14, 1972	2229:27.8	6.29	144.45	5.9	5.5	197	RM
3	Nov. 1, 1972	2122:15.3	6.35	144.41	5.6	4.9	162	RM
4	Sept. 6, 1977	0852:29.5	6.11	143.20	5.5	5.6	153	HRVa
			Eastern Irian Jaya					
5	Feb. 19, 1970	2255: 4.4	4.50	140.03	5.6		119	
6	June 25, 1976	1918:57.4	4.58	140.14	6.3	7.1	425	RM
7	June 27, 1976	1912:29.8	4.52	140.24	5.9	5.6	266	
8	July 17, 1976	0532:41.2	4.56	139.95	5.7	5.5	232	RM
9	Oct. 29, 1976	0251: 7.3	4.54	139.93	6.0	7.1	409	RM
10	Jan. 19, 1981	1510:59.9	4.56	139.28	6.0	6.7	359	RM,L,HRVb
11	Dec. 2, 1982	1936:57.7	4.55	138.95	5.6	5.2	218	HRVc
			West Highlands					
12	March 9, 1969	1348: 1.3	4.10	135.65	5.6	6.6	186	JM
13	April 17, 1973	1234:27.3	4.32	134.26	5.7	6.4	307	
14	Nov. 18, 1976	0543:41.4	4.25	135.14	5.7	6.2	256	
15	Jan. 8, 1979	0727: 0.7	4.15	135.99	5.4	5.3	137	HRVd
16	April 8, 1985	1915:14.2	4.10	136.28	5.8	5.9	311	HRVe
17	Sept. 15, 1985	0129:23.3	4.12	136.25	5.5	6.3	314	HRVf
18	Sept. 15, 1985	0242:54.5	4.09	136.07	5.7	6.4	394	HRVf

Locations, magnitudes, and number of recording stations from the ISC catalog.

[a] From NEIC catalog before 1978.

[b] Number of stations used to locate the earthquake.

[c] Previously published focal mechanisms are abbreviated by author: RM, Ripper and McCue [1983]; JM, Johnson and Molnar [1972]; L, Letz [1985]; HRVa, Dziewonski et al., [1987a]; HRVb, Dziewonski and Woodhouse [1983]; HRVc, Dziewonski et al. [1983]; HRVd, Dziewonski et al. [1987b]; HRVe, Dziewonski et al. [1986a]; HRVf, Dziewonski et al. [1986b]. "HRV", centroid-moment tensor solutions, rest are first-motion focal mechanisms.

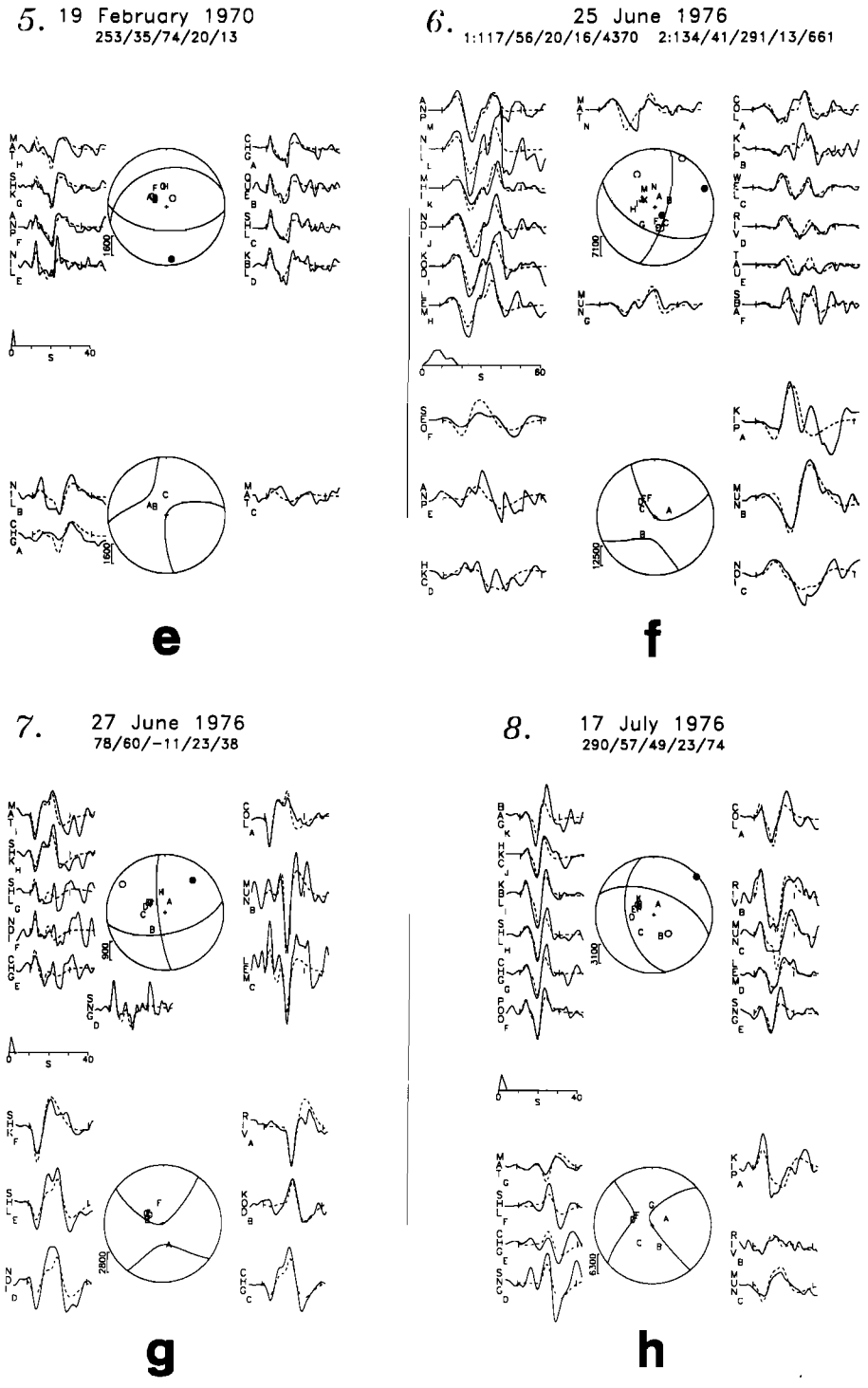

Fig. 3. (continued)

(Figures 3a and 5). These arrivals are clear on all seismograms (Figure 3a) and are the first strong arrivals following the direct P, making it unlikely that the depth phases arrive any earlier. Changing the depth of the event by as little as 1.3 km produces observable differences in timing of the depth phases (Figure 5). Thus, for a given crustal velocity structure, depths can be determined to within 1 to 2 km using short-period waveforms. The depth decreased by 0.9 km when the structure was assumed to be a half-space with sedimentary velocities, suggesting that errors in depth due to assuming the wrong velocity structure are near 1 km. We conclude that the event is within 2-3 km of 11 km depth and is below the 5 km depth to the detachment.

Other PNG earthquakes. Events 2 and 3 (Figures

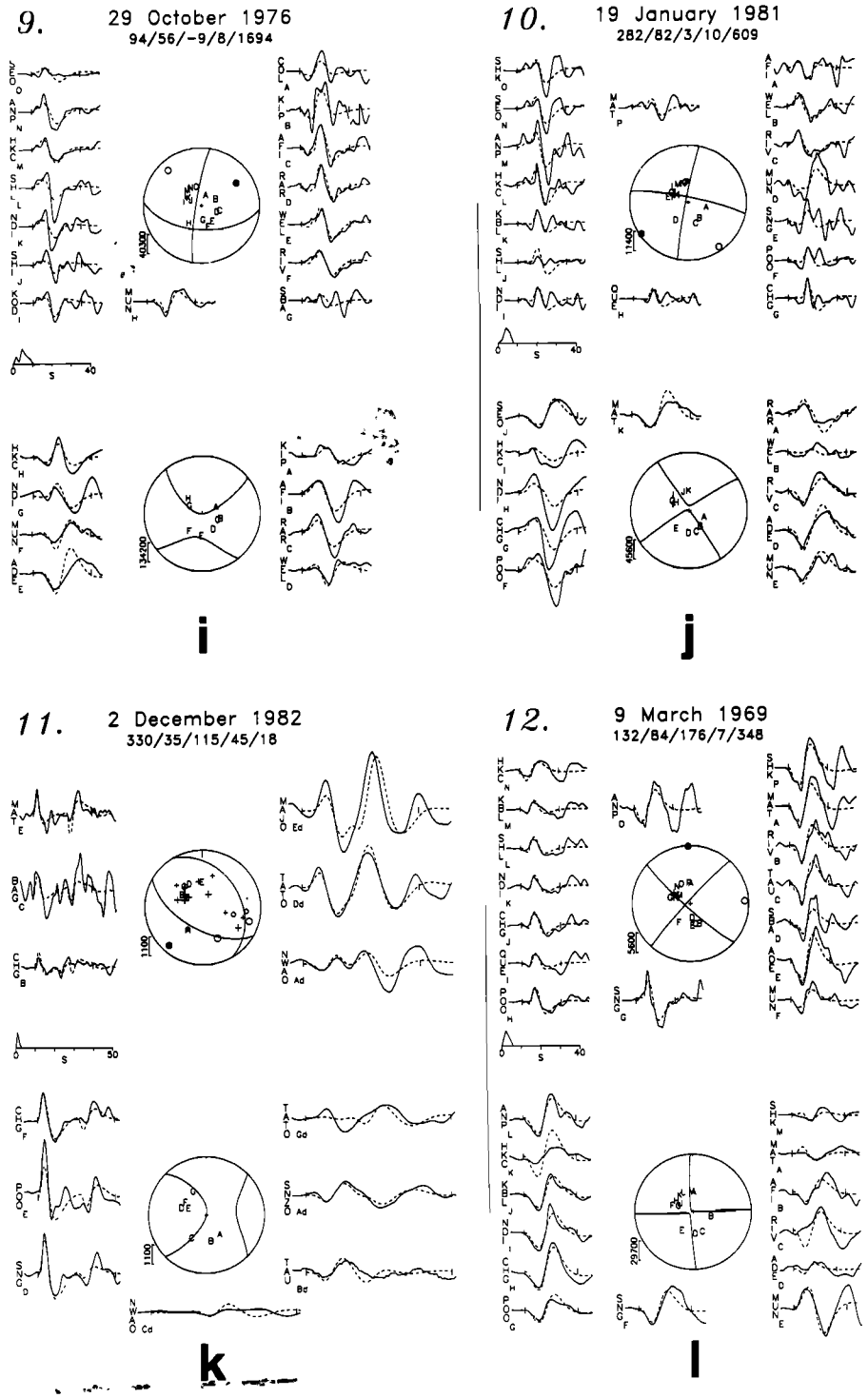

Fig. 3. (continued)

3b and 3c) were located 10-20 km south of the Kubor Uplift (Figure 4) and exhibit high-angle thrusting at 20-25 km depth. Nodal planes strike parallel to local structural trends and have orientations similar to those found by Ripper and McCue [1983]. Event 2 was large enough to be recorded by stations covering a wide range in azimuth and its mechanism is well constrained by the waveforms. Analysis of other well-recorded events with similar mechanisms and depths suggests that the uncertainties are 5 km or less in depth and 10°-15° in mechanism orientation (see appendix). Event 3 was smaller (Table 1) and was recorded only by high-gain stations to the northwest, spanning 28° in azimuth. Consequently, the mechanism is not as well-constrained as that for event 2, but the similarity of the available waveforms to those for event 2 indicates a similar mechanism and depth (see appendix).

Event 4 (Figure 3d) was located west of events

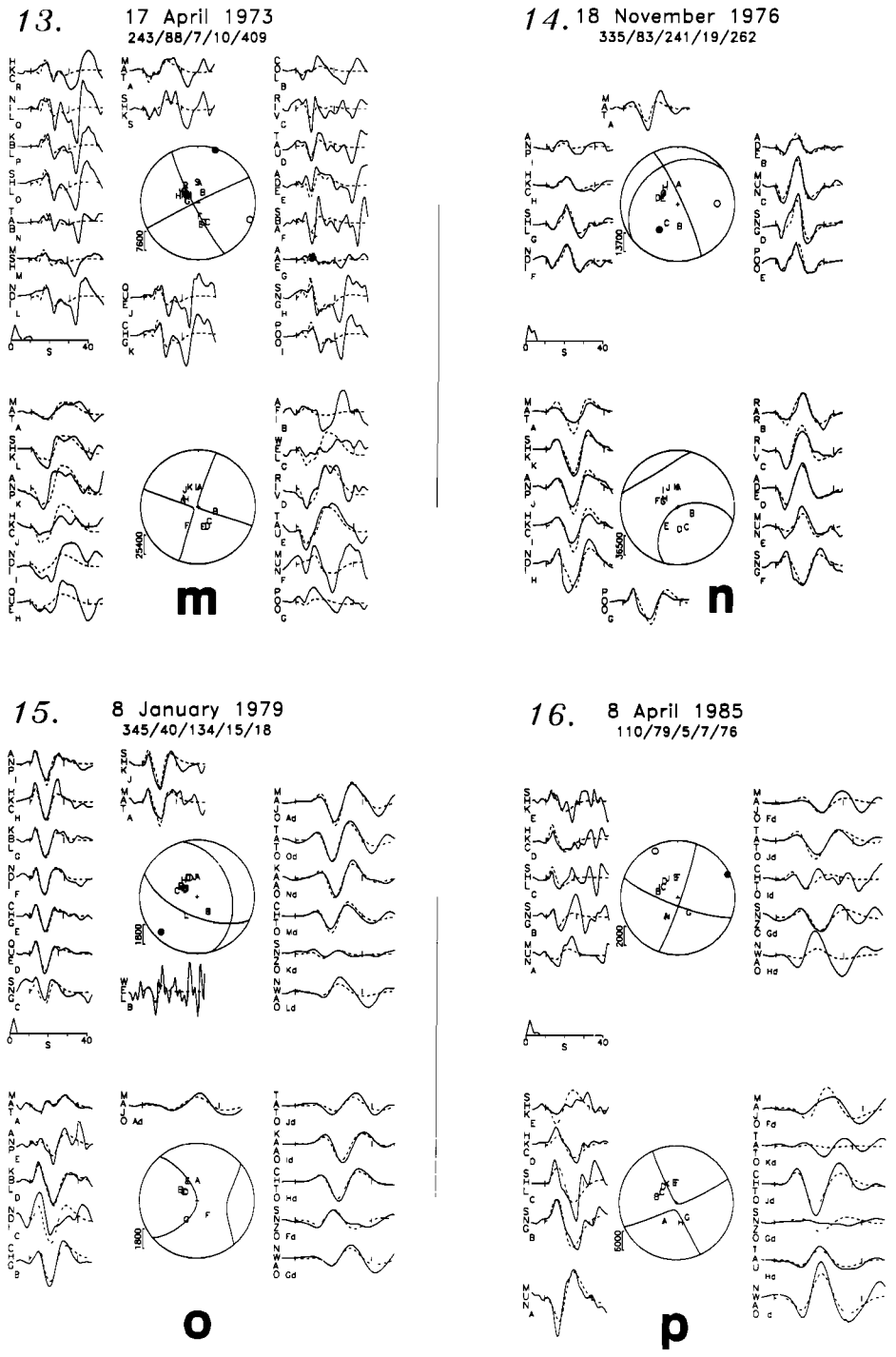

Fig. 3. (continued)

1-3, beneath the flanks of the Quaternary Kerewa volcano (Figure 4), and caused landslides near the town of Margarima [Davies, 1983; Ripper and McCue, 1983]. This is the only thrust earthquake presented in this paper that has a depth of less than 10 km and is probably within 2 km of the surface. A shallow source is indicated by the narrowness of the initial half cycle of the P wave, caused by truncation due to the arrival of reflected phase pP of opposite polarity. The truncation of the first half cycle is not due to the termination of the source-time function because the second and third half cycles are broader, requiring a source duration of about 7 s. Small P-to-SH amplitude ratios for a thrust mechanism are also diagnostic of a shallow depth. Because the reflected pP phase and the direct P phase interfere destructively for this mechanism, while the reflected and direct SH phases interfere constructively, P-to-SH amplitude ratios decrease observably as the source comes within a few kilometers of the surface. For

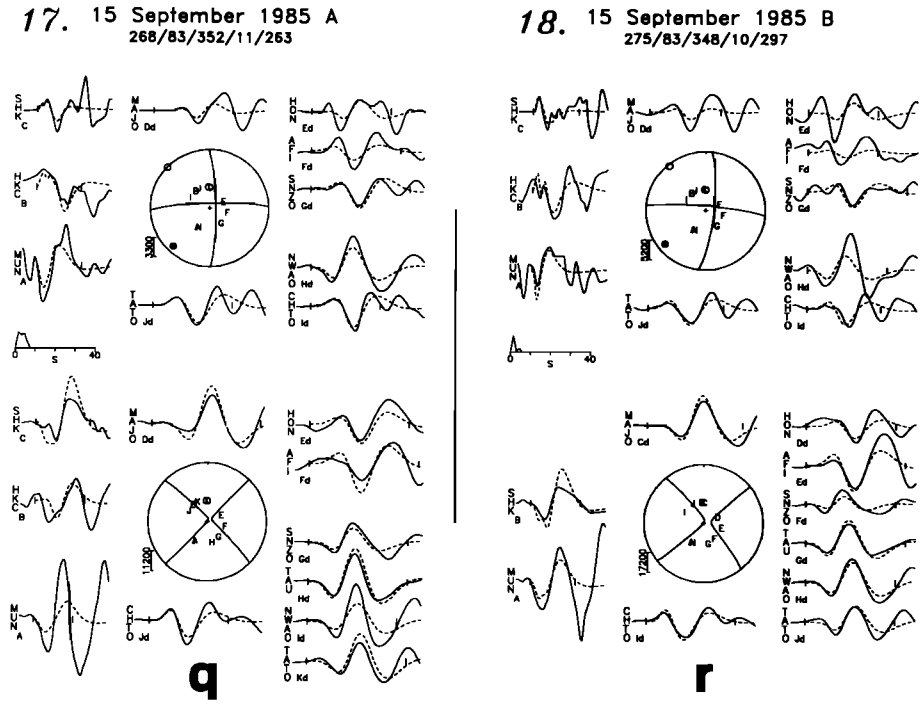

Fig. 3. (continued)

example, compare SH/P amplitudes for events 3 and 4 (note amplitude scale at bottom left of SH and P focal spheres).

Earthquakes in Eastern Irian Jaya

The three largest earthquakes in the Highlands ($M_b \geq 6.0$) occurred in eastern Irian Jaya between 139°E and 140.5°E, along with numerous aftershocks (Figure 2). The seven events discussed in this section form an east-west linear trend 150 km long and 10 km wide that is parallel to surface structures west of 139.6°E but cuts across structures east of 139.6°E (Figure 6). The ISC epicenters are between 0 and 30 km south of the highest parts of the ranges, where elevations exceed 4000 m, and are between 20 and 55 km from the foreland basin, which is at sea level. First-motion solutions by Ripper and McCue [1983] and Letz [1985] are considerably different from our mechanisms for events 6, 8, and 10, but similar for event 9. While the centroid-moment tensor solutions for events 10 and 11 are similar to ours [Dziewonski and Woodhouse, 1983; Dziewonski et al., 1983].

Although three small events, 5, 8, and 11, have high-angle thrust mechanisms similar to earthquakes in PNG, the three largest and one small earthquake have strike slip mechanisms. (The normal faulting mechanism on Figures 1 and 6, discussed below, is a subevent of the largest strike-slip earthquake, event 6.) The east-west striking nodal planes of the strike-slip events are parallel to both the alignment of epicenters and nearby structural trends, suggesting that they are the fault planes. The sense of motion on the strike-slip faults is therefore left lateral (see Discussion). Strike-slip earthquakes 6a, 7, and 9 show fault planes that dip south at 55°-60°.

Earthquakes 5 and 8 show high-angle thrusting at 20-25 km depth and shortening roughly perpendicular to the mountain chain. Azimuthal station coverage is poor for event 5, and uncertainties in the mechanism are probably larger than for other thrust events (appendix). The depth for event 8 is determined by the clear reflected phases, suggesting ±5 km depth uncertainty (Figure 8). Event 11 shows thrusting at 45 km depth, in the lower crust or uppermost mantle, with the mechanism constrained to agree with first motions picked by us from both WWSSN records and seismograms recorded at stations in PNG (Figure 3k).

June 25, 1976 (Event 6). This was the largest earthquake in the Highlands since the WWSSN was installed (M_s = 7.1; M_0 = 5 x 10^{19} N m) and caused extensive surface damage, deaths, and injuries [Ripper and McCue, 1983]. Aftershocks persisted for at least half a year and include three other events studied here (7, 8, and 9). The waveforms from the main shock (Figures 3f and 7) show a complex series of arrivals at all stations. Smaller events in the same area (5, 7, and 8) have simpler waveforms and are matched with point source mechanisms in half-space source structures (Figures 3e, 3g, and 3h), demonstrating that the additional arrivals observed from the June 25, 1976 event are likely produced by the earthquake source rather than by near-source structure.

For the main shock an arrival 20 s after the first arrival can be seen on almost all records and is interpreted as a second subevent. Initially the waveforms were fit with a single mechanism and a source time function 36 s long (Figure 7, case I). The resulting mechanism is

TABLE 2. Summary of Results

Event	Depth, km	MO, 10^{17} N m	T95[a], s	Plane 1 Strike	Plane 1 Dip	Plane 1 Rake	Plane 2 Strike /Dip	P axis Azimuth /Plunge	T axis Azimuth /Plunge	Number of Waveforms P	Number of Waveforms SH	VAR/ pwr[b]
					Papua New Guinea							
1	11.3±0.2	1.9± 0.2	0.9±0.2	276± 3	51± 1	85±1	104/39	10/ 6	156/83	13	2	0.530
2	22.9±1.3	3.5± 0.2	3.0±0.6	248± 5	45± 1	80±2	83/46	166/ 1	70/83	11	6	0.343
3	21.0±2.4	1.0± 0.1	1.3±1.3	259± 8	59± 2	80±6	99/32	357/14	143/73	6	4	0.377
4	0.5±0.2	14.6± 2.2	6.8±2.7	0± 5	41±12	114±6	149/53	253/ 6	3/73	10	9	0.303
					Eastern Irian Jaya							
5	19.6±0.7	1.3± 0.1	1.6±1.0	253±11	35± 3	74±6	93/56	175/11	36/76	8	3	0.382
6a	16.3±1.8	437.4±39.1	15.3±3.6	117± 4	56± 4	20±3	15/73	69/11	331/36	14	6	0.347
6b[c]	13.4±3.9	66.2±24.8	6.7±10.3	134±12	41± 4	291±8	287/52	140/75	29/ 5	14	6	0.347
7	23.0±0.0	3.8± 0.4	2.1±1.1	78± 5	60± 4	-11±2	174/81	40/28	303/14	9	6	0.242
8	22.6±1.0	7.4± 0.5	3.2±1.0	290± 4	57± 2	49±3	168/51	48/ 3	143/56	11	7	0.296
9	8.1±2.2	169.5±18.6	8.8±3.3	94± 2	56± 6	-9±4	189/83	57/29	317/18	15	8	0.335
10	10.2±1.7	58.0± 9.0	4.4±2.1	282± 3	82± 2	3±2	191/87	236/ 3	146/ 8	16	11	0.391
11	44.6±1.2	1.8± 0.1	2.3±0.8	330± 1	35± 0	115±0	120/59	222/12	352/71	6	7	0.417
					West Highlands							
12	7.4±1.3	34.8± 3.6	4.7±2.4	132± 2	84± 2	176±2	223/86	358/ 2	88/ 7	16	13	0.255
13	9.8±1.3	40.9± 7.2	11.6±5.6	243± 3	88± 3	7±2	153/83	18/ 4	108/ 6	19	12	0.465
14	19.2±1.1	26.2± 2.4	5.2±1.8	335± 3	83± 2	241±7	233/30	216/44	89/32	9	11	0.170
15	15.4±0.7	1.8± 0.1	1.8±1.2	345± 3	40± 1	134±3	114/62	225/12	338/61	16	11	0.214
16	6.8±3.9	7.6± 1.4	6.3±5.5	110± 3	79± 6	5±5	19/86	65/ 4	334/11	11	11	0.371
17	11.3±3.0	26.3± 4.3	6.2±4.5	268± 4	83± 4	352±3	359/82	223/11	314/ 1	10	11	0.340
18	9.6±1.7	29.7± 3.2	4.9±2.4	275± 3	83± 3	348±3	6/78	230/13	321/ 3	10	10	0.361

Uncertainties are twice the standard errors.

[a] T95 is source duration, calculated from second moment of source time function.

[b] Weighted misfit variance/weighted power in data.

[c] Second subevent of event 6 is delayed 15.0±0.8 s and is shifted 2.1±5.7 km at 148±20° from the epicenter of event 6a.

oblique slip and does not match observed seismograms from most stations south and east of the epicenter. The match is much better (23% decrease in variance) when the earthquake is broken into two subevents with different mechanisms (Figure 7, case IV). The first subevent had a strike-slip mechanism and 87% of the total seismic moment (Figure 7, case II) and was followed 20 s later by a smaller, predominantly normal-faulting subevent (Figure 7, case III). The first subevent shows more impulsive arrivals to the NW than to the SE and is matched by a small component of thrusting. The strikes of the nodal planes for the second subevent are unconstrained because the calculated P waves are very similar at all azimuths and SH arrivals for this subevent cannot be identified with confidence.

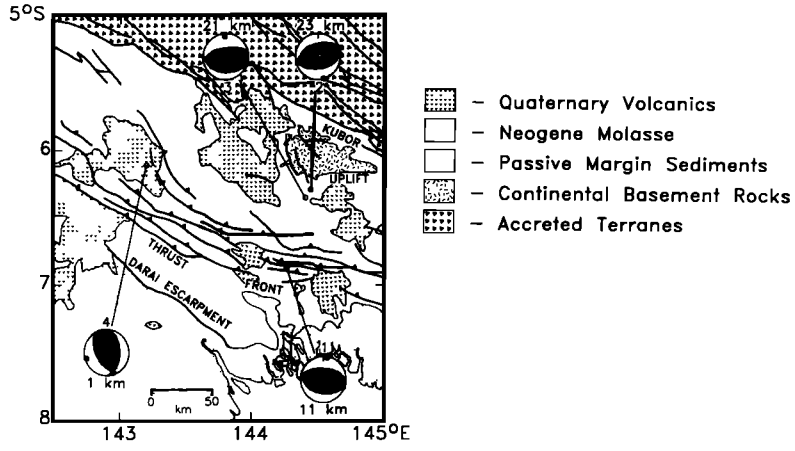

Fig. 4. Map showing focal mechanisms and geological structures in PNG, near Events 1-4. Geology is generalized from D'Addario et al. [1976]. Event numbers and depths (labelled in km) are shown next to the focal spheres. Focal spheres plotted in the same format as in Figure 2, except that the sizes are not scaled to seismic moment. Also shown are patterns representing different groups of tectonic units.

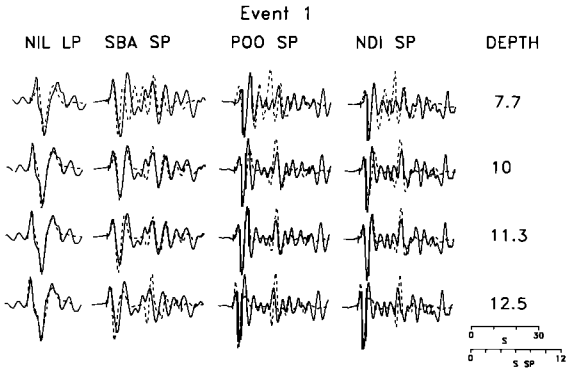

Fig. 5. P wave seismograms at different depths for event 1. Depths are marked in kilometers at the right. Solid lines are observed seismograms and dashed lines are calculated, assuming a source structure with 9 km of sediments overlying a half-space as discussed in the text. The waveforms at 7.7 km depth represent the best fit when the source is constrained to be in the sedimentary layer but clearly do not match the observed seismograms. Instrument types are marked as "LP" or "SP" for long-period and short-period instruments, respectively. Seismograms for different instruments have different time scales, shown at lower right, with "S SP" designating the short-period time scale.

Depth of faulting. The large strike-slip earthquakes have best fit centroid depths less than 20 km, while the thrust earthquakes are deeper than 20 km (Table 2). The smallest strike-slip event, event 7, has a depth of 23 km and does not fit this pattern, but the three large events, 6, 9, and 10, have depths of 16, 8, and 10 km, respectively. The thrust earthquakes, 5, 8, and 11, have respective depths of 20, 23, and 45 km. In order to assess the vertical relationship between the large strike-slip events and the thrust events, calculated waveforms were fit to the observed seismograms for one strike-slip and one thrust earthquake while fixing the depth at each of a range of values (Figure 8). The two events are located 3 km apart by the International Seismological Centre, Edinburgh (ISC) (Figure 6, Table 1), so that near-source velocity structure should be the same and differences in waveforms should reflect only differences in mechanism and depth.

For the thrust earthquake all P and some SH waveforms (e.g., MAT) are matched closely at depths between 20 and 25 km (Figure 8, top). Observed waveforms for the large strike-slip earthquake are matched equally well at all depths shallower than 10 km but are fit poorly at 20 km depth (Figure 8, middle). The increase in variance with depth for the strike-slip event (Figure 8, bottom) shows a broader minimum than for the thrust event. For both earthquakes, visually acceptable matches to waveforms are found at depths whose variance is within 10% of the minimum, corresponding to uncertainties of 7-8 km in depth for the strike-slip earthquake and 3 km in depth for the thrust. Thus strike-slip event 9 has a depth less than 15 km while thrust event 8 is between 20 and 25 km deep, and the strike-slip earthquake is resolvably shallower than the thrust. The allowable depth ranges will change if errors in the velocity structure are present, but the depths of the events will stay proportionally the same.

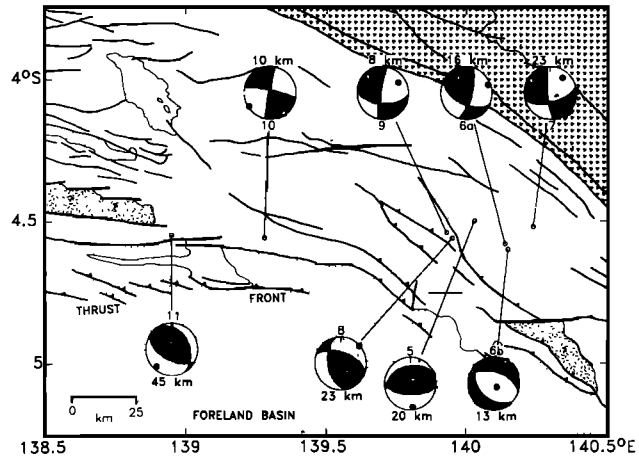

Fig. 6. Map showing focal mechanisms and geological structures in east Irian Jaya, near events 5-11. Geology generalized from Dow et al. [1986]. Symbols are the same as for Figure 4.

Earthquakes in the West Highlands

The remaining seven earthquakes are at the western end of the mountain ranges, at the western limit of autochthonous Australian continental crust. Earthquake mechanisms indicate both thrust and strike-slip faulting in a linear seismic zone between 4.1°S and 4.3°S (Figure 9). Westward along this zone, thrust-belt structures give way to a complex zone of left-lateral shear between the presumably left-lateral Tarera and

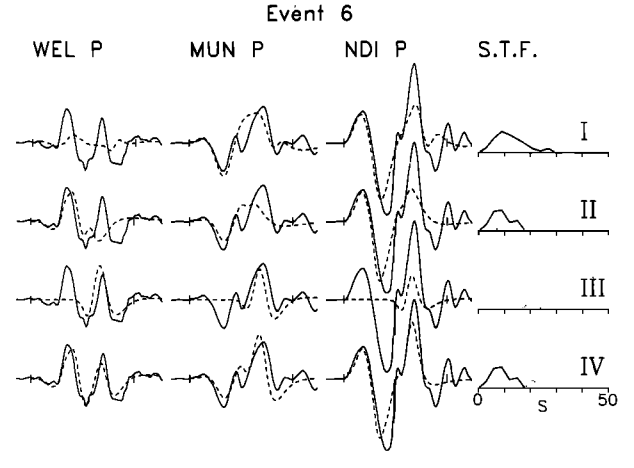

Fig. 7. Selected observed (solid) and calculated (dashed) seismograms for different mechanisms for event 6. The source-time function is shown at the right with the time scale for seismograms; the source-time function for the second subevent is shown by dotted lines. Case I: Single event, source-time function is 36 s long. II-IV: Double event. Case II: first subevent only (strike-slip mechanism). III: second subevent only (normal faulting mechanism). IV: both subevents and resulting waveform.

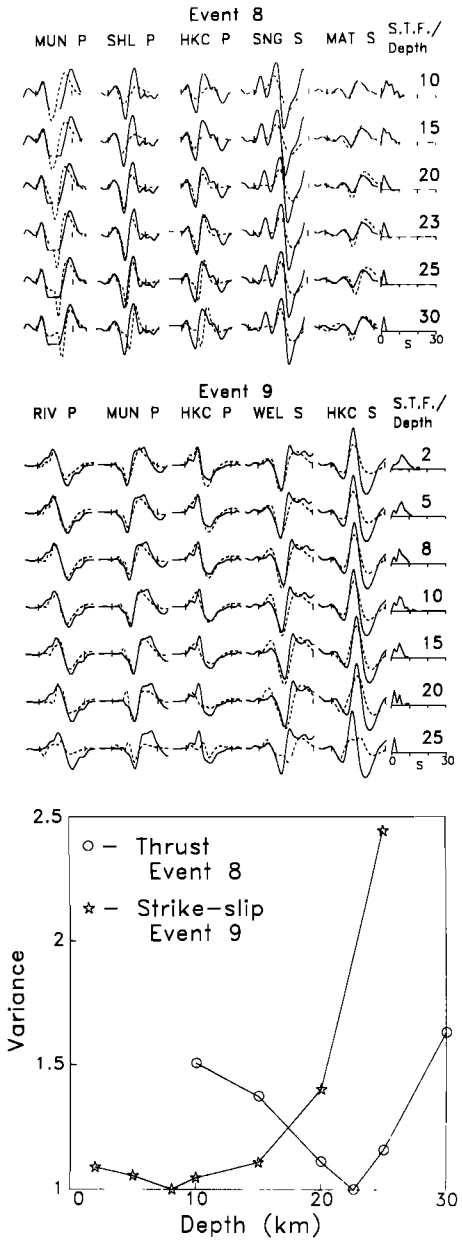

Fig. 8. (Top) Waveforms at different depths for a thrust earthquake, event 8. (Middle) Waveforms at different depths for a strike-slip earthquake, event 9. (Bottom) Variance at each depth shown above, for the thrust earthquake and for the strike-slip earthquake. Variances are normalized to the minimum value for each event. Depths are indicated in kilometers on the right, with the source-time function.

Aiduna faults [Dow and Sukamto, 1984a; Hamilton, 1979; Visser and Hermes, 1962].

Five earthquakes showed strike-slip mechanisms that are generally consistent with left-lateral slip on east-west striking fault planes, although strikes vary from 110° in the east (event 16) to 43° in the west (event 12). Johnson and Molnar [1972] used P-wave first motions to determine a nearly identical mechanism to ours for event 12, and centroid-moment tensor solutions for events 16-18 agree with our solutions [Dziewonski et al., 1986a, b]. Event 12, with a strike of 223°, is located where the Aiduna fault has a more northeast strike, and the orientation of this mechanism may reflect a bend in the fault zone, although the mapped fault trace is not parallel to either nodal plane (Figure 9). If the earthquake is mislocated, then it may show left-lateral slip on a splay fault mapped 20 km southwest of the reported epicenter. Strike-slip mechanisms for events 16, 17, and 18 show that left-lateral faulting continues east of the mapped faults. Event 13 may be evidence for an active offshore extension of the Aiduna fault zone, but an unusually high ISC standard deviation for arrival times for this event (3.64 s instead of 1.0-2.5 s for the other events) and systematic arrival time residuals determined from the alignment of observed and synthetic waveforms suggest that it may be considerably mislocated. Relocation using travel times determined from the waveform alignments in Figure 3m results in a 75 km northward shift of the epicenter.

Other events in this area include a small high-angle thrust (event 15, $M_0 = 2 \times 10^{17}$ N m) and a moderate-sized earthquake showing either strike-slip or dip-slip faulting (event 14, $M_0 = 3 \times 10^{18}$ N m). Because analog records with clear arrivals for the thrust event (event 15) are only available at a small range of azimuths, the depth is less reliable than those of most other thrusts (see Appendix). Event 14 is interpreted as showing either dip-slip motion on the near-vertical nodal plane with the west side rising relative to the east or as left-lateral strike-slip motion on a fault plane dipping 30° to the northwest. The ISC location is within 5 km of the Aiduna fault and the northwest dipping nodal plane strikes parallel to the surface fault trace. If the shallow-dipping plane is the fault plane, then event 14 shows left-lateral motion on a strike-slip fault, possibly the Aiduna fault, dipping at an unusually low angle 19 km below the surface. Alternatively, the choice of the other

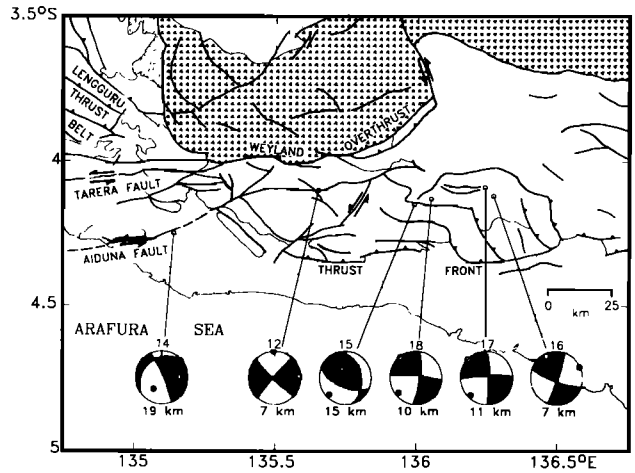

Fig. 9. Map showing mechanisms and geological structures in west Irian Jaya, near events 12-18 (event 13 is farther west and is not shown). The geology is generalized from Dow et al. [1986] and Pigram and Panggabean [1983]. Symbols are the same as for Figure 4.

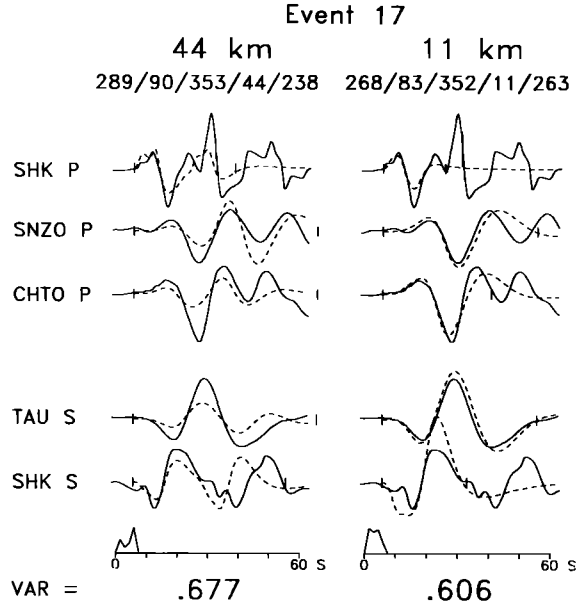

Fig. 10. (Left) Best fit for event 17 determined by inversion when the observed large arrival 20-30 s after the first arrival is assumed to be a depth phase. The resulting depth is 44 km. (Right) Best fit when the late phase is not included in the inversion and the depth phase is assumed to arrive within 15 s of the direct phase. Note that the vertical tics indicate the inversion window for each seismogram. Variance is shown at bottom, normalized by power in the seismograms, calculated in both cases within the windows used for the deeper solution (left).

nodal plane as the fault plane implies that vertical dip-slip faulting is present, possibly below the strike-slip fault zone along a fault striking perpendicular to the Aiduna fault.

A large unmatched phase is observed 20-30 s after the first P arrival and some SH arrivals for the five strike-slip events; it is largest for events 13, 17, and 18 (Figures 3m, 3q, 3r, and 10). Because this phase is present in many events, it is unlikely to be caused by source complexities but is either a free surface reflection unmatched because of grossly incorrect depths or an arrival produced by unmodeled structures. The first possibility is tested by placing event 17 at 45 km, aligning the observed late phase with the computed depth phases, and inverting for all source parameters, including depth. The mechanism remains strike slip and the depth moves to 44 km, but the waveforms fit poorly and the timing of the late phase is not matched at many stations: SH waveforms are particularly poorly matched (Figure 10). The shallower solution is visually more consistent with the observed waveforms and shows 10% smaller variance. We suggest that the late phases are produced by lateral variations in structure. Because a strike-slip mechanism radiates the largest P amplitudes horizontally, rays that are bent toward the vertical by unmodeled variations in velocity will produce large arrivals on observed seismograms. Even gently dipping (1°-3°) planar reflectors can produce late large arrivals for strike-slip earthquakes [e.g., Langston, 1977; Wiens, 1987].

Discussion

Depth of thrust earthquakes and detachment faulting. The eight thrust earthquakes show that active, steeply dipping thrust faults extend to midcrustal depths. If the north dipping nodal planes are the fault planes, as suggested by the dips of thrust faults observed on the surface, then the dip angles of active fault planes range from 35°-60°. Except for event 4 all the thrust earthquakes are below the sedimentary section (11 to 45 km depth). The depths and steep fault planes demonstrate that the active deformation is not confined to be above a shallow-dipping detachment within the sediments [Findlay, 1974; Jenkins, 1974] but instead extends to midcrustal depths.

Detachment thrusts are assumed to exist in Papua New Guinea (PNG) below the Tertiary carbonate sequence, in the Jurassic sequence [Findlay, 1974; Jenkins, 1974] or in Cretaceous siltstones [Dow, 1977; Hobson, 1986]. The depth to the décollement, on the basis of seismic, drilling, and gravity observations, is 3-5 km in the southern part of the thrust belt, becoming deeper northward to 10-15 km, as the detachment steps down to lower structural levels and the sedimentary section thickens [Findlay, 1974; Hobson, 1986]. Detachments have been mapped at similar structural levels at the extreme western end of the Highlands [Pigram and Panggabean, 1983], but little surface information is available for the rest of Irian Jaya. Thin-skinned structures are exposed and documented best in PNG, so the discussion on style of thrusting will concentrate on the eastern part of the Highlands.

Event 4 is within 2 km of the surface and appears to show faulting of the sediments above the detachment. This earthquake is located under the slopes of a large Quaternary volcano (Figure 4) and may be caused by magmatic intrusion related to volcanism rather than by crustal shortening due to regional compression. Its nodal planes are nearly parallel to nearby north-northwest trending faults and folds that also exist far from the volcanic center, suggesting that the mechanism orientation is controlled by tectonic rather than volcanic factors.

The remaining three earthquakes in PNG have east-west striking nodal planes, parallel to nearby thrusts and folds despite having depths well below assumed depths to detachments. Events 2 and 3 show high-angle thrusting at 20-25 km depth north of the region of pronounced thin-skinned thrusting, at the southern flank of the Kubor Uplift (Figures 4 and 11a). The causative faults might be connected to shallow detachment thrusts in the sediments and may form a steep downdip extension of the shallow thrusts (Figure 12). The earthquakes provide a mechanism for accommodating some shortening in the basement that in the sediments is taken up along the detachment. In order for the detachment to reach events 2 and 3 (Figures 11a and 12) the thin-skinned part of the thrust belt can be only ~50 km wide and restricted to the lower mountains south of the earthquakes (1 km mean elevation).

Event 1 is beneath the frontal thrusts in PNG

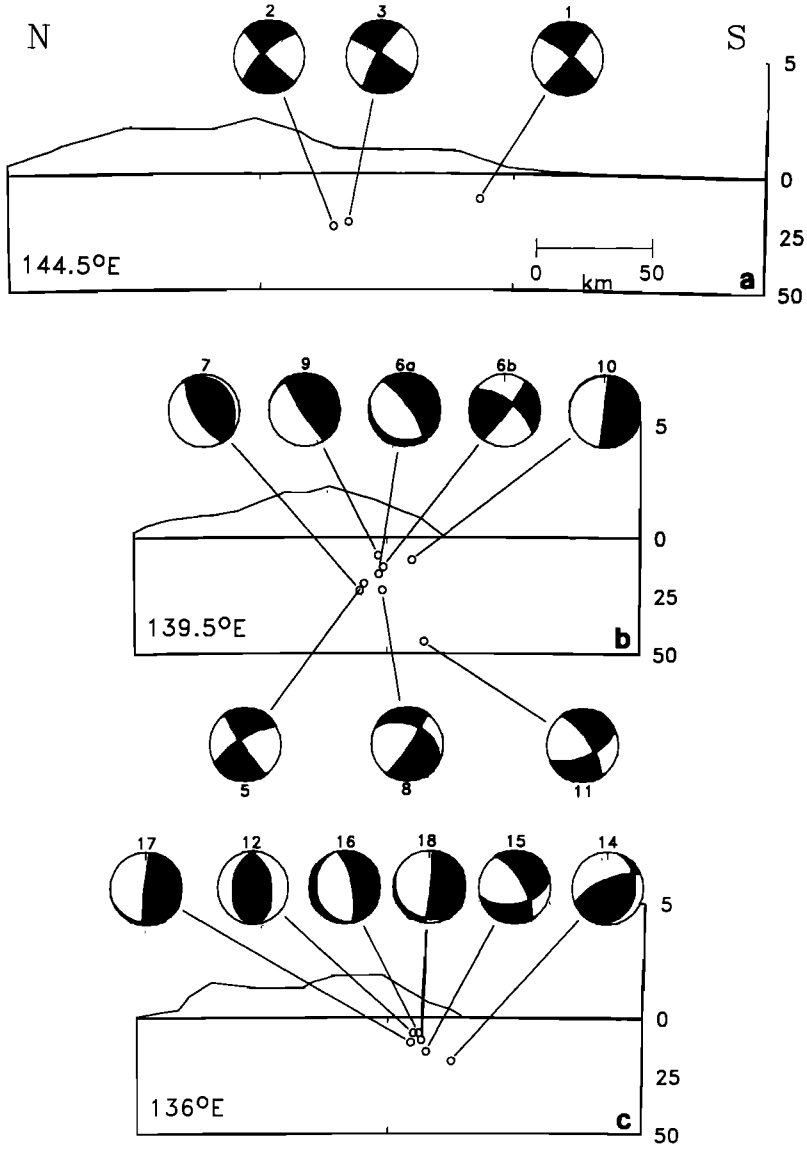

Fig. 11. Cross sections of seismicity and topography: a, b, and c refer to the profile locations on Figure 2. Vertical exaggeration is 10x for topography and 1x for seismicity, as indicated by the vertical scale bars on right. Horizontal scale, indicated on profile a, is the same for all profiles. Focal spheres are plotted as back hemisphere projections, and compressional quadrants are filled.

and shows that active basement deformation occurs beneath the thrust belt as far south as does thin-skinned faulting. Its 11-km depth places it in the uppermost basement, or possibly in the lowermost sediments, but well below the 3-5 km depth of the detachment surface. Cross sections interpreted from seismic lines often show high-angle faults with small offsets in the basement (0.5-1 km) beneath the detachment fault in many parts of the frontal thrust system [Jenkins, 1974]. The Darai Escarpment 50 km south of the thrust front is suspected to be a high-angle thrust extending into the basement, on the basis of the broad curvature of the 1-km-high plateau, lack of stratigraphic repetition in drill holes, and gravity measurements over the escarpment [e.g., Anfiloff and Flavelle, 1982; Hobson, 1986; Jenkins, 1974]. Other broad, deeply rooted folds suggestive of basement faulting may exist south of the frontal thrusts in Irian Jaya [Silver and Smith, 1983]. Event 1 apparently shows thrusting on such a feature in PNG, beneath the frontal thrusts, implying that high-angle basement faults contribute to the total shortening beneath the mountain belt.

The relationship between the detached thin-skinned thrust belt and the deeper high-angle thrusting earthquakes at the northern edge of the thin-skinned belt is similar to relationships between thrust belts and large earthquakes in other active thrust belts, such as the Peruvian sub-Andes [Suárez et al., 1983] and the Tadjik basin in central Asia [Abers et al., 1988]. In both these thrust belts the largest earthquakes are located toward the hinterland from the detachment zone at the foot of the high mountains

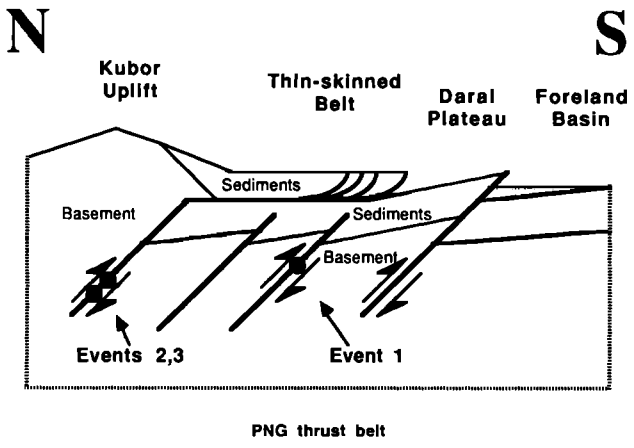

Fig. 12. Cartoon showing how thin-skinned faulting mapped in PNG might be related to faulting in the basement, inferred from the earthquakes and other evidence discussed in the text. See Figure 11a for comparison to actual topography and earthquake mechanisms.

(High Andes and Hindu Kush), and the earthquakes show high-angle thrusting at midcrustal depths. However, the presence of large strike-slip earthquakes near the thrusts in Irian Jaya and high-angle thrusts immediately beneath the detached thrust belt in PNG (i.e., event 1) show that analogies between faulting in New Guinea and elsewhere are not very straightforward.

The north dipping nodal planes for the crustal thrust events in Irian Jaya (events 5, 8, and 15) dip near 45° and project to the surface near the active thrust front (Figures 6, 9, and 11). Because the thrust earthquakes in Irian Jaya are within 25-50 km of the thrust front, the average dips of thrust faults must be quite high if they are on downdip continuations of the faults observed at the range front; the steep average dips probably preclude detachment faulting. It is conceivable that there are low-angle thrusts in the foreland basin, largely buried by the foreland sediments and not associated with observable topography, although the molasse basin is fairly thin (0.5-2 km) [APC, 1961; Visser and Hermes, 1962]. Nevertheless, the thrust belt which is thin skinned in PNG (Figure 4) does not seem to be present in much of Irian Jaya, but, instead, thrusts appear to be steep over considerable depth ranges, perhaps similar to Laramide thrusting observed in the Wind River Range of Wyoming [Smithson et al., 1979]. Thus, while it is common to draw analogies between the New Guinea fold-and-thrust belt and older thin-skinned thrust belts such as the Canadian Rockies or the southern Appalachians [e.g., Hobson, 1986; Jenkins, 1974; Pigram and Panggabean, 1983], it may be equally appropriate to draw analogies between the New Guinea thrust belt and thick-skinned belts such as the Wyoming and Colorado Laramide ranges [Silver and Smith, 1983].

Strike-slip faulting. Although thrust faulting undoubtedly plays an important role in building the New Guinea Highlands, the largest earthquakes have strike-slip mechanisms and show that the mountains in Irian Jaya are undergoing significant left-lateral shear. There is a large gap without recent large earthquakes between 136.3°E and 138.9°E, but narrow belts of seismicity (5-15 km wide by 150 km long) occur 20-55 km from the mountain fronts in eastern and western Irian Jaya. These earthquakes demonstrate active left-lateral strike-slip faulting within the thrust belt on faults parallel to the mountain front.

The geometry of the seismic zone is more consistent with an east-west, left-lateral fault zone than with right-lateral slip on north-south fault planes. Source durations up to 20 s for the largest earthquakes (Table 2) imply fault segments 25-100 km long, depending on rupture geometry. These fault lengths are longer than would be expected for north-south tear faults, unless such tear faults run the entire width of the mountain belt. In eastern Irian Jaya, where the largest earthquakes occurred, aftershock epicenters are within 20 km of 4.5°S latitude over a 120 km distance along strike, consistent with an east-west fault zone (Figures 2, 6, and 11). Also, surface lineaments trend west or northwest throughout much of the area and the medial suture north of the thrust belt is not offset, suggesting that strike-slip faults do not trend north. Right-lateral faulting may be

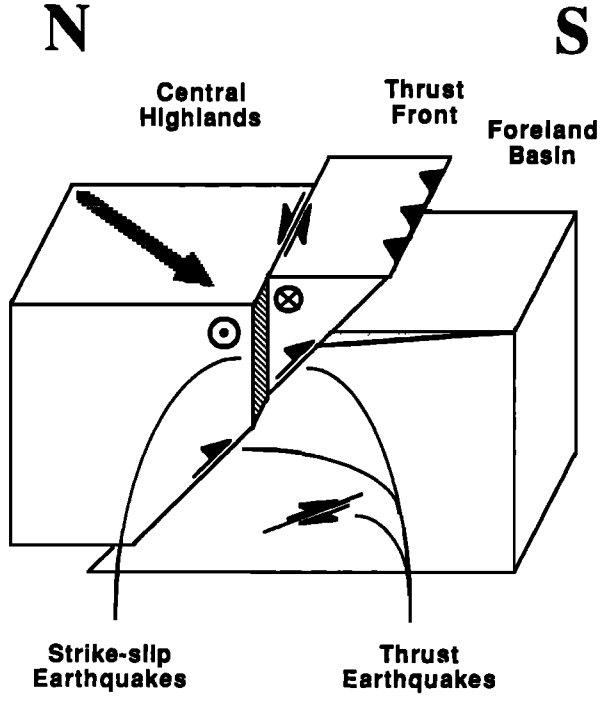

Fig. 13. Schematic block diagram showing how strike-slip and thrust faulting might be related in Irian Jaya, modified from Fitch [1972]. Oblique convergence, indicated by the shaded arrow, is occurring along oblique-slip thrust faults north of the strike-slip fault and by decoupled strike-slip and thrust faulting farther south. Although many observations are not explained by this simple mechanism, it accounts for the observed locations and depths of strike-slip and thrust earthquakes and for the recent thrusting at the range front.

arguable for some of the earthquakes in western Irian Jaya where a wider variety of structural and earthquake mechanism orientations are observed, but here, too, the large earthquakes are restricted to a 10 to 15-km-wide by 200-km-long east-west trending belt.

Hence we argue that the large earthquakes are evidence for an east-west striking left-lateral shear zone. The zone is 20-55 km north of the range fronts, just south of the highest topography, and extends throughout Irian Jaya and possibly into PNG. There are suggestions from surface geology that left-lateral motion occurs in the west Highlands: Using satellite imagery, Dow and Sukamto [1984b] identified streams offset left laterally across one major fault; Hamilton [1979] inferred left-lateral shear from left-stepping anticlines and thrust faults in the southern foothills (Figure 6); and Carey [1958] identified structures in the foreland related to wrench faulting. Nevertheless, there are no mapped left-lateral strike-slip faults in the region of the epicenters for the strike-slip earthquakes (Figure 6), perhaps because mapping in eastern Irian Jaya has been done largely from aerial photographs, on which strike-slip faults may be difficult to identify in mountainous regions. Furthermore, large landslides that may cover active fault traces accompanied the three largest earthquakes studied here as well as some of the smaller earthquakes [Ripper and McCue, 1983; H. Letz, personal communication, 1986;]. (To our knowledge, no fault scarp associated with a recorded earthquake has ever been found in New Guinea.) The strike-slip faults on which these earthquakes occurred may reach the surface but, not surprisingly, have not been mapped because of the lack of sufficient field work and the difficulty in identifying such features in mountainous, jungle-covered regions. It seems likely that in older mountain belts, strike-slip faulting may have accompanied thrusting but has gone unnoticed because of the difficulty of identifying it in the geologic record.

Relationship of strike-slip to thrust faulting. An unusual aspect of the earthquakes is the apparent juxtaposition of thrust and strike-slip faulting within the thrust belt in Irian Jaya. Both types of faulting occur south of the highest parts of the mountains, 20-55 km north of the range front (Figures 6, 9, and 11). We have shown that the thrust events are resolvably deeper than the strike-slip events. The apparent exception, event 7 with a strike-slip mechanism at 23 km depth, is the smallest, the farthest east, and the farthest from the range front of the strike-slip events. Generally, active faulting seems to be restricted to the southern part of the mountains, with shallow strike-slip earthquakes just south of the highest peaks and thrust earthquakes deeper than the strike-slip events. Active thrust faults are also observed at the range front south of the strike-slip events. The separation of strike-slip faulting from the thrust faulting both below and to the south of it demonstrates decoupling of strike-slip and dip-slip motions.

The Highlands are advancing southward over a steeply dipping ramp while strike-slip faulting cuts the upper plate (Figure 13). The active part of the mountains forms a wedge bound on the south by the active thrust front and on the north by the strike-slip faults inferred from the earthquakes. This wedge is apparently moving south with respect to the foreland basin and east with respect to northern New Guinea. The actual distribution of faults is admittedly more complex than shown in Figure 13, and the modes of faulting are probably not completely decoupled (as indicated by left-stepping thrusts at the range front).

This geometry is similar to that proposed for transcurrent fault zones parallel to volcanic arcs, such as Sumatra, Japan, and the Philippines, and their adjacent subduction zones [Fitch, 1972], although in New Guinea the strike-slip faults reach the surface only 20-55 km from the range front, rather than a few hundred kilometers from a trench. The decoupling geometry proposed for these subduction zones appears to explain observations of active faulting in New Guinea. Compression near strike-slip fault zones is more often associated with thrust faults that steepen with depth and merge with the strike-slip fault rather than cutting the strike-slip fault at depth [e.g., Lowell, 1972]. Such a geometry is not viable here because thrust earthquakes are observed immediately below the strike-slip events and their nodal planes do not steepen near the strike-slip fault.

The proposed configuration of strike-slip and thrust faults is geometrically unstable with time. The strike-slip fault zone is limited to the hanging wall of the thrust and is being thrust onto the foreland. All faults are rotating both by left-lateral shear and south vergent shear due to thrusting. For example, the south dip of fault planes for strike-slip events 6, 7, and 9 may be due to rotation of the strike-slip fault planes along the thrust faults. As the mountains evolve, both the thrust faults and the strike-slip faults will advance southward, gradually incorporating more of the foreland. Alternatively, it may be that strike-slip faulting in the thrust belt is a recent phenomenon and the present geometry of active faulting is transitional. Either scenario could explain Davies's [1982] observation of early Neogene south vergent thrusting followed by later strike-slip faulting in the Mobile Belt in westernmost PNG.

Eastward extension of strike-slip faulting. The largest earthquakes show strike-slip faulting in eastern Irian Jaya, and moderate-sized earthquakes show left-lateral slip on an east-west fault zone west of the large earthquakes. Because no large events were found in the thrust belt in PNG between 1964 and 1985, it is difficult to know whether or not the strike-slip fault zone extends to the east. At least two earthquakes with magnitude $M \geq 7.0$ occurred in the PNG part of the thrust belt in this century (Figure 2, inset), but well-constrained focal mechanisms have not been determined for them. In 1954 a shallow, magnitude 7.0 earthquake was located at 5.5°S, 142.5°E, and in 1922 a magnitude 7.5 event extensively damaged the coastal region at the eastern extremity of the thrust belt [Everingham, 1974; Ripper and McCue, 1983]. It is not clear that events 1-4 represent the dominant mode of faulting in PNG; it is conceivable that an active strike-slip fault zone exists in the fold belt, perhaps producing large infrequent earthquakes such as those earlier in

this century. Considerable lateral offset has been suggested on faults immediately north of the thrust belt, in the medial suture zone [e.g., Davies, 1978; Dow, 1977].

The change in regional strike of the thrust belt at 140°E may be partly responsible for the lack of strike-slip activity in the east, and thrust faulting may be the predominant mode of deformation in PNG. West of 140°E the thrust belt strikes east-west, while east of that longitude the mountain belt bends ~45° and strikes northwest-southeast (Figure 1), more perpendicular to plate convergence. With this geometry, pure thrust faulting in PNG and a combination of thrust and strike-slip faulting in Irian Jaya can result from the same net convergence direction, ~N45°E. This direction is perpendicular to many thrust structures in PNG and parallel to the P axes of most strike-slip earthquakes in Irian Jaya. Deformation north of the thrust belt, such as in the Bismark Sea or in northern New Guinea, could account for the difference between the N45°E direction and the direction of convergence between the Pacific plate and Australia (N70°E).

Rates of deformation from seismic moments. The seismic moments of the earthquakes provide an estimate of the rate of slip on strike-slip faults in the fold-and-thrust belt [Brune, 1968]. Such estimates do not account for aseismic slip and earthquakes other than those studied here and are based on a short time period, so they should be interpreted with caution. Because the strike-slip earthquakes appear to lie on a single plane, we assume that they represent slip on a single fault. The average fault slip is given by $\bar{u} = \sum M_0/(\mu A)$, where A is the total fault area, $\sum M_0$ is the sum of the seismic moments for strike-slip earthquakes, and μ is the shear modulus [Brune, 1968]. The strike-slip fault zone in Irian Jaya is 500-800 km long (from 134° or 136°E to ~141°E) and extends to 20-25 km depth (the depth of the thrust earthquakes), giving a fault area A = 1-2 x 10^{10} m^2. The summed seismic moment of the strike-slip earthquakes is ~10^{20} N m with roughly a 20% uncertainty (Table 1), and we use $\mu = \rho V_s^2 = 3.3 \times 10^{10}$ N/m^2, giving $\bar{u}$ = 0.15-0.30 m. Since we are examining earthquakes over 22 years, the average rate of strike-slip faulting across the thrust belt is 7-14 mm/a. Taking into account reasonable uncertainties of our estimates of the seismic moments, the seismic slip rate is probably in the range 5-20 mm/a. Smaller earthquakes not considered here ($M < 5.5$) probably account for another ~19% of the total seismic moment (following Chen and Molnar [1977], assuming that we are sampling all earthquakes with $5.5 \leq M \leq 7.1$), although we do not know how many of these earthquakes have strike-slip mechanisms. Thus the rate of east-west left-lateral motion suggested by the strike-slip earthquakes is 5-25 mm/a, compared to a total of ~100 mm/a for the east-west component of slip between the Pacific plate and Australia predicted by plate motions.

The slip rate calculated here is only meaningful if the earthquakes in the 22-year period studied are typical of activity over longer time spans. The largest earthquakes in this century in the western fold-and-thrust belt (Figure 2) are a magnitude 7.8 event on October 7, 1900 at 4.0°S, 140.0°E, near the 1976 sequence, a magnitude 7.1 event in 1942 in Irian Jaya at 4.5°S, 135.0°E, and events 6 and 9 (M_S = 7.1 for both) [Everingham, 1974; Ganse and Nelson, 1981]. If the assigned magnitudes for the 1900 and 1942 events are roughly correct, then they correspond to about 5 to 10 M=7.1 events in terms of seismic moment. In this case the moment release per 10 years is roughly equivalent to one M=7.1 earthquake, as we have witnessed over the last 22 years.

Estimates of convergence rates from crustal thickening. The crustal thickening needed to create the topography of the Highlands gives an estimate of the total amount of crustal shortening (Figure 14). We assume that prior to collision the area that is now the Highlands was near sea level (suggested by shallow-water marine facies of Miocene sediments [Dow, 1977]) and the crust was 30 km thick (suggested by refraction and shear wave studies in the foreland basin and Arafura Sea [Bowin et al., 1980; Brooks, 1969; Finlayson, 1968]). In order to estimate its crustal thickness we assume that the Highlands are presently compensated by a crustal root, with crust and mantle densities of 2800 and 3300 kg/m^3, respectively. These assumptions implicitly ignore many thermal, compositional, and to some extent flexural influences on topography that would bias our estimates of Moho depth. We further assume that crustal volume is conserved during collision and material is not transferred along strike, so that the cross-sectional area of the crust in each profile remains constant during collision. This last assumption neglects the

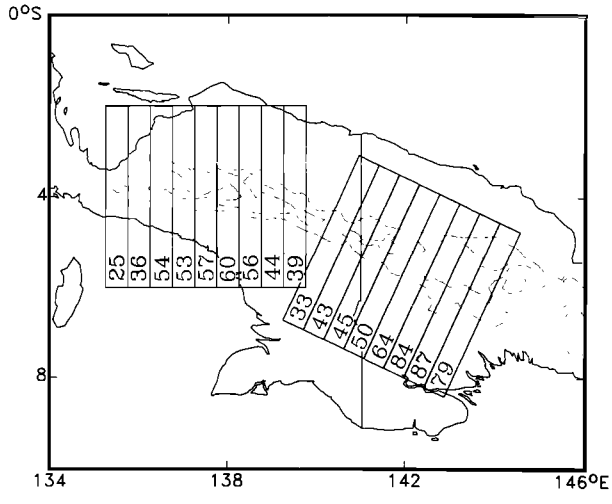

Fig. 14. Estimates of crustal shortening from topographic height of the Central Highlands, for each of a series of profiles. Numbers are the estimates of shortening in kilometers along each profile, assuming topography is isostatically compensated by a crustal root and that the initial crustal thickness is 30 km. Crustal volume is assumed to remain constant along each profile as the mountains form so that the total cross-sectional area of crust along each profile is the same before and after collision. Topography is contoured every 1000 m above sea level (dotted lines), from Heirtzler [1985].

potentially large effects of subduction of crust, strike-slip faulting, and magmatic additions to the crust. Erosion should have a small influence on these estimates; even if we assume that a crustal volume equivalent to the existing topography has already been eroded, the shortening estimates would increase by only 17%. The total shortening along each profile is then given by integrating the excess crustal thickness over the width of the mountains and dividing by the original crustal thickness.

Using 5-min topographic averages [Heirtzler, 1985], we measured the cross-sectional area of the Highlands topography on 17 profiles perpendicular to the mountain fronts (Figure 14). The shortening estimates varied from 87 km over the Kubor uplift to 33 km near 140°E and 25 km near 135°E, averaging 61 km east of 140°E and 47 km to the west. These estimates suggest that the region around the Kubor uplift has experienced nearly twice as much shortening as regions to the east. From palinspastic reconstructions, Hobson [1986] estimated 75 km of shortening in the sediments south of Kubor area, compared to ~30 km of shortening in western PNG. Despite the potentially large errors associated with our estimates they are within 30% of Hobson's values for shortening in the sediments and show similar along-strike variations. The coincidence of the values is somewhat surprising and may be fortuitous, both because Hobson did not consider strike-slip faulting or basement shortening (indicated by earthquake depths) and because most of the assumptions in our estimates, mentioned above, are associated with potentially large errors.

If all the crustal thickening occurred in the last 10 m.y., suggested by the initiation of clastic sedimentation in the foreland basin, then the average convergence rate is 4-9 mm/a. However, if the northern parts of mountains started forming 30 Ma, when the first collisions with the Australian continent occurred [e.g. Pigram and Davies, 1987], then the average convergence rate is 1 - 3 mm/a. These rates are likely underestimates, as material has been eroded off the mountains and some lithosphere may have been subducted after collision took place. The rates are comparable to, although considerably less than, the rate of the north-south component of Pacific-Australia convergence (~50 mm/a).

Implications for Australia-Pacific convergence. The above estimates, from seismic moments and topography, shows that 5 to 20% of the total convergence between the Pacific plate and Australia is probably taken up in the fold-and-thrust belt. In particular, some of the strike-slip component of convergence is accounted for here. The strike-slip earthquakes in the Highlands, together with the Sorong fault in the northwest [Dow and Sukamto, 1984a] and active transforms in the Bismark sea in the northeast [Taylor, 1979] can account for all of the east-west left-lateral motion, and additional zones of strike-slip faulting are not required. Deformation in northern New Guinea, suggested by large earthquakes not studied here, may be as important as deformation in the fold-and-thrust belt. The shortening in the mountains seems insufficient to account for all of the convergence in New Guinea.

Conclusions

Thrust faults in the New Guinea fold-and-thrust belt extend into the basement at high angles. Basement-involved thrusting is found as far south as the frontal thin-skinned thrusts and may account for a substantial amount of the shortening in the thrust belt.

The largest earthquakes in the thrust belt are in Irian Jaya and show strike-slip faulting. The probable fault planes strike east-west, along which left-lateral slip occurs. The strike-slip earthquakes are located within 55 km of the thrust front and can be traced east from the offshore Tarera-Aiduna fault in the Banda Sea east to at least the PNG border at 141°E. High-angle thrust earthquakes are found below the strike-slip earthquakes, at 20-25 km depth, indicating that strike-slip faulting is restricted to the upper plate. Seismic moments of the strike-slip earthquakes reveal slip rates of 5-25 mm/a and can explain some of the difference between the direction of Pacific-Australia plate motion and the strike of fold-and-thrust structures in New Guinea.

Crustal thicknesses of the mountains in New Guinea, inferred from topography and isostasy, imply 35-90 km of convergence across the mountains and show that some, but probably not all, of the motion between the Pacific plate and Australia is absorbed in the fold-and-thrust belt. Crustal shortening and strike-slip faulting in the New Guinea Highlands probably represent 5-20% of the total motion between the Pacific plate and Australia.

Appendix: Uncertainties in Waveform Inversion

Uncertainties in source parameters. Because formal errors significantly underestimate true uncertainties [e.g., Nábělek, 1984], it is necessary to have other measures of the quality of the results. Our strategy is to fix the parameter to be examined at successive values and to determine the remaining source parameters by waveform inversion. The resulting matches between calculated and observed waveforms are inspected visually and statistically to determine acceptable ranges for the parameter being investigated (e.g., Figures 5, 8, and A1). Solving for all other parameters allows tradeoffs to be explored, for example, between mechanism and depth (Figure A1) or between depth and source duration (Figure 8). This empirical approach to estimating uncertainties provides the acceptable ranges of parameters for a given event and can be used to infer uncertainties for other events with similar mechanisms and depths, although results are strictly applicable only to the event examined.

Several studies have shown that depths can be determined to within 1-10 km using body waveform inversion [e.g., Abers et al., 1988; Huang et al., 1986; McCaffrey and Nábělek, 1987; Nábělek, 1984; Nelson et al., 1987]. Tests in this paper (Figures 5 and 8) show that depths of dip-slip New Guinea earthquakes have uncertainties of 5 km or less. Depths for strike-slip earthquakes usually are more difficult to constrain mainly because the P and pP phases have small amplitudes, making arrival times difficult to pick, and because P and sP have the same

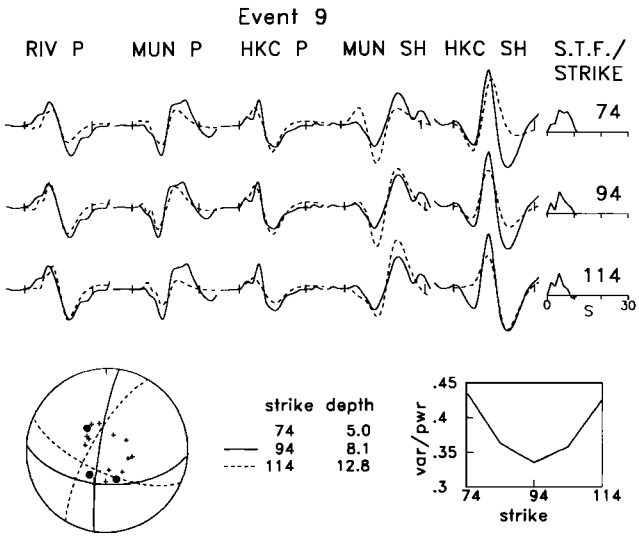

Fig. A1. (Top) Selected seismograms for event 9 with the strike fixed at three different values. (Bottom) Mechanisms, depths, and variances with the strike fixed at each value. Variance is shown at lower right, normalized by the total power in the waveforms. The stations shown, RIV, MUN, and HKC, are shown as solid circles on the focal sphere, and other stations used in the inversion are shown by plus signs. Strike is given in degrees, and depth is in kilometers.

polarity, making depth phases more difficult to identify. These features result in tradeoff between depth and source time function. For example, Figure 8 shows that seismograms from one large strike slip earthquake can be matched over a range of depths nearly twice as large as that for a nearby small thrust.

McCaffrey and Nábělek [1987] and Abers et al. [1988] showed that orientation of nodal planes for moderate-sized thrust earthquakes can be determined to within 10°-15° when station coverage is good, although this requires reliable SH waveforms when both planes dip near 45°. P waves for strike-slip events are quite sensitive to mechanism orientation, as shown for seismograms for event 9 (Figure A1). Here, the strike of the probable fault plane is varied between 74° and 114°, but acceptable fits are found only for strikes between 84° and 104°. The dip of the fault plane varies considerably with the strike (28°-68°), as do the depth (5-13 km) and moment (19-13 x 10^{18} N m), demonstrating considerable coupling between parameters.

Effects of irregular station distribution. The distribution of stations around New Guinea is highly irregular, and we test here its influence on the inversion results. Almost all high-gain WWSSN stations within 90° of New Guinea are in Asia and so are restricted to the northwest quadrant of the focal sphere. Commonly we obtain usable seismograms from stations in south Asia and Australia only, and sometimes only from Asia. For events with $M_0 < 10^{18}$, 83% of all analog records are from stations in the northwest quadrant, while for larger events, 59% of the analog records are from these stations. High-gain digital stations exist to the south and are used whenever available to provide more uniform station coverage for the smaller events.

We tested the effect of sparse and uneven station distributions by solving for the parameters of one well-constrained thrust, event 8, with various subsets of stations (Figure A2). In case I we used 7 seismograms (SNG, SHL, HKC, and MUN P, and SNG, HKC, and MUN SH), including only one station (MUN) to the south. Inversion of these waveforms at different depths showed a similar minimum in variance at the same depth as inversion using all 18 seismograms (Figure A2). There were no significant changes in the other parameters between case I and the inversion of all waveforms (differences are +0.3 km in depth, +7° in strike, +1° in dip, -5° in rake, and -0.5x10^{17} N m in moment). In case II (Figure A2)

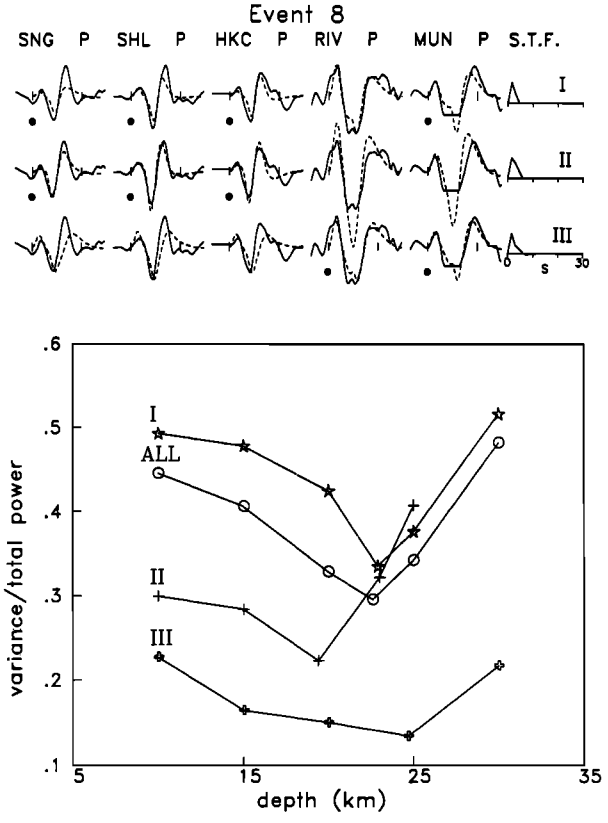

Fig. A2. Station distribution test using seismograms for Event 8. (Top) Observed (solid) and calculated (dashed) P waves at best depth determined by the inversion for each subset of stations. Solid dots indicate stations used in each inversion (SH waves were also used for each station shown except SHL). Source-time function is shown at right with time scale for seismograms. (Bottom) Variance divided by power in waveforms as a function of depth, for solutions using different sets of stations. "ALL" corresponds to case when all seismograms were used, shown in Figures 3h and 8. I, II, and III correspond to cases using only the stations indicated at top. At each depth, other parameters were determined to produce closest match between observed and calculated seismograms. Stations SNG, SHL, and HKC are northeast of the earthquake, and RIV and MUN are south of the earthquake.

we removed station MUN so that all three stations were to the northwest. In this case the depth decreased by 3.5 km from case I, and the moment increased by 7.4×10^{17} N m, while the mechanism remained relatively fixed (changes in mechanism from case I to case II are +0° in strike, -6° in dip, and -4° in rake). The shape of the variance-depth curve was similar in case I and case II, but the minimum-variance depth decreased in case II. In a final test, case III (Figure A2), we inverted P and SH seismograms from only the two Australian stations, MUN and RIV. The depth increased from case I to case III by 2.2 km, and the variance-depth curve showed a broader variance minimum. These tests show that it is not necessary to have a large number of stations but that it is important to have some stations at widely spaced azimuths. In particular, stations at different azimuths can have different timing between direct and reflected phases which will indicate different depths. Depth phases are later at stations to the south than to the northwest, causing the depth determined from Australian stations only (case III) to be 5-6 km deeper than that determined from Asian stations only (case II).

Strong azimuthal variations can be caused by rupture propagation [e.g., Ben-Menahem, 1961], but such effects are unlikely to be apparent for this event because of the short (3-4 s) source duration, since variations for the pP-P times of 1-2 s are necessary to explain the discrepancy in depths. It is more likely that the observed change in pulse width with azimuth is caused by azimuthal variations in velocity structure, either near the source or elsewhere along the raypaths. The travel time variations may be due to the velocity contrast between the low-velocity basin sediments to the south and the high-velocity ultramafic rocks to the north. A deep sedimentary basin on one side of an earthquake in the Tien Shan probably causes similar variations in travel times for depth phases [Nelson et al., 1987].

These tests show that limited station coverage can bias depth estimates by ~5 km. Events 3 and 5 have no seismograms outside of the northwest quadrant, while events 4 and 11 only have digital seismograms, which are less sensitive to source depth than are WWSSN seismograms, in other quadrants. If the variations observed in seismograms for event 8 are produced by near-source structure, then the calculated depths for 3 and 5 may be underestimated by 3-4 km. Events 3 and 5 are within 10 km of events 8 and 2, respectively, and have similar mechanisms. The 3-km difference between events 5 and 8 and the 2 km difference between events 3 and 2 are not significant.

Acknowledgments. Our understanding of New Guinea tectonics benefitted greatly from discussions with numerous workers at the Bureau of Mineral Resources, Australia, the Geological Research and Development Centre, Indonesia, and the Port Moresby Geophysical Observatory, Papua New Guinea. We thank Hugh Davies, Chris Pigram, Rab Sukamto, and Horst Letz for copies of their unpublished and hard-to-find papers and Steve Roecker for an insightful review. John Nábělek and Eric Bergman helped us with aspects of the waveform analysis. G. Abers acknowledges support from an NSF Graduate Fellowship. This research was funded by NSF grant EAR-8608405.

References

Abers, G. A., C. Bryan, S. W. Roecker, and R. McCaffrey, Thrusting of the Hindu Kush over the Tadjik Basin, Afghanistan: Evidence from two large earthquakes, Tectonics, 7, 41-56, 1988.

Aki, K., and P. G. Richards, Quantitative Seismology, Theory and Methods, 557 pp., W. H. Freeman, San Francisco, Calif., 1980.

Anfiloff, V., and A. J. Flavelle, Formal gravity interpretation over the 800-m Darai escarpment in New Guinea, Geophysics, 47, 1091-1099, 1982.

Australasian Petroleum Co. (APC), Geological results of petroleum exploration in western Papua, J. Geol. Soc. Aust., 8, 1-133, 1961.

Bain, J. H. C., D. E. Mackenzie, and R. J. Ryburn, Geology of the Kubor Anticline, central highlands of Papua New Guinea, Bull. Bur. Miner. Resour. Geol. Geophys. Aust., 155, 1975.

Ben-Menahem, A., Radiation of seismic surface waves from finite moving source, Bull. Seismol. Soc. Am., 51, 401-435, 1961.

Bowin, C. O., G. M. Purdy, C. Johnston, G. G. Shor, L. Lawver, H. M. S. Hartono and P. Jezek, Arc-continent collision in the Banda Sea region, Am. Assoc. Pet. Geol. Bull., 64, 868-915, 1980.

Brooks, J. A., Rayleigh waves in southern New Guinea, II, A shear velocity profile, Bull. Seismol. Soc. Am., 59, 2017-2038, 1969.

Brune, J. N., Seismic moment, seismicity, and rate of slip along major fault zones, J. Geophys. Res., 73, 777-784, 1968.

Carey, S. W., The tectonic approach to continental drift, in Continental Drift -- A Symposium, edited by S. W. Carey, pp. 177-355, Tasmania University, Hobart, 1958.

Chen, W. P., and P. Molnar, Seismic moments of major earthquakes and the average rate of slip in Central Asia, J. Geophys. Res., 82, 2945-2969, 1977.

Cooper, P., and B. Taylor, Seismotectonics of New Guinea: A model for arc reversal following arc-continent collision, Tectonics, 6, 53-67, 1987.

D'Addario, G. W., D. B. Dow, and R. Swoboda, Geology of Papua New Guinea, 1:2,500,000 map, Bur. of Miner. Resour. Aust., Canberra, 1976.

Davies, H. L., Geology and mineral resources of Papua New Guinea, paper presented at 3rd Regional Conference on Geology and Mineral Resources of Southeast Asia, Bangkok, 1978.

Davies, H. L., Mianmin, Papua New Guinea, scale 1:250,000 Geol. Ser.-Explanatory Notes, Geol. Surv. of Papua New Guinea, Port Moresby, 1982.

Davies, H. L., Wabag, Papua New Guinea, scale 1:250,000 Geol. Ser.-Explanatory Notes, Geol. Surv. of Papua New Guinea, Port Moresby, 1983.

Dewey, J. F., and J. M. Bird, Mountain belts and the new global tectonics, J. Geophys. Res., 75, 2625-2647, 1970.

Doutch, H. F., Plate tectonic map of the Circum-Pacific region, Southwest Quadrant, Am. Assoc. of Pet. Geol., Tulsa, Okla, 1981.

Dow, D. B., A geological synthesis of Papua New

Guinea, Bull. Bur. Miner. Resour. Geol. Geophys. Aust., 201, 41 pp., 1977.
Dow, D. B., and R. Sukamto, Western Irian Jaya: the end product of oblique plate convergence in the late Tertiary, Tectonophysics, 106, 109-139, 1984a.
Dow, D. B., and R. Sukamto, Late Tertiary to Quaternary tectonics of Irian Jaya, Episodes, 7, 3-9, 1984b.
Dow, D. B., G. B. Robinson, U. Hartono, and N. Ratman, Geologic map of Irian Jaya, Indonesia, 1:1,000,000 scale, Geol. Resour. Dev. Centre, Indonesia, Bandung, 1986.
Dziewonski, A. M., and J. H. Woodhouse, An experiment in systematic study of global seismicity: Centroid-moment tensor solutions for 201 moderate and large earthquakes of 1981, J. Geophys. Res., 88, 3247-3272, 1983.
Dziewonski, A. M., A. Friedman, D. Giardini, and J. H. Woodhouse, Global seismicity of 1982: Centroid-moment tensor solutions for 308 earthquakes, Phys. Earth Planet. Inter., 33, 76-90, 1983.
Dziewonski, A. M., J. E. Franzen, and J. H. Woodhouse, Centroid-moment tensor solutions for April - June, 1985, Phys. Earth Planet. Inter., 41, 215-224, 1986a.
Dziewonski, A. M., J. E. Franzen, and J. H. Woodhouse, Centroid-moment tensor solutions for July - September 1985, Phys. Earth Planet. Inter., 42, 205-214, 1986b.
Dziewonski, A. M., G. Ekström, J. E. Franzen, and J. H. Woodhouse, Global seismicity of 1977: Centroid-moment tensor solutions for 471 earthquakes, Phys. Earth Planet. Inter., 45, 11-36, 1987a.
Dziewonski, A. M., G. Ekström, J. E. Franzen, and J. H. Woodhouse, Global seismicity of 1979: Centroid-moment tensor solutions for 524 earthquakes, Phys. Earth Planet. Inter., 48, 18-46, 1987b.
Everingham, I. B., Large earthquakes in the New Guinea-Solomon islands area, 1873-1972, Tectonophysics, 23, 323-338, 1974.
Findlay, A. L., The structure of foothills south of the Kubor Range, Papua New Guinea, APEA J., 14, 14-20, 1974.
Finlayson, D. M., First arrival data from the Carpentaria region upper mantle project (CRUMP), J. Geol. Soc. Aust., 15, 33-50, 1968.
Fitch, T. J., Plate convergence, transcurrent faults and internal deformation adjacent to southeast Asia and the western Pacific, J. Geophys. Res., 77, 4432-4460, 1972.
Futterman, W. I., Dispersive body waves, J. Geophys. Res., 67, 5279-5291, 1962.
Ganse, R. A., and J. B. Nelson, Catalog of Significant Earthquakes 2000 B.C. - 1979, Including quantitative casualties and damage (with supplement), 154 pp., World Data Cent. A for Solid Earth Geophys., NOAA, Boulder, Colo., 1981.
Giardini, D., A. M. Dziewonski, and J. H. Woodhouse, Centroid-moment tensor solutions for 113 large earthquakes in 1977-1980, Phys. Earth Planet. Inter., 40, 259-272, 1985.
Hamilton, W., Tectonics of the Indonesian region, U.S. Geol. Surv. Prof. Pap., 1078, 1-345, 1979.
Heirtzler, J. R. (Ed.), Digital relief of the surface of the earth, report, Nat. Geophys. Data Cent., Boulder, Colo., 1985.
Hobson, D. M., A thin skinned model for the Papuan thrust belt and some implications for hydrocarbon exploration, APEA J., 26, 214-224, 1986.
Huang, P. Y., S. C. Solomon, E. A. Bergman, and J. L. Nábělek, Focal depths and mechanisms of Mid-Atlantic Ridge earthquakes from body waveform inversion, J. Geophys. Res., 91, 579-598, 1986.
Jackson, J., Errors in focal depth determination and the depth of seismicity in Iran and Turkey, Geophys. J. R. Astron. Soc., 61, 285-301, 1980.
Jenkins, D. A., Detachment tectonics in western Papua New Guinea, Geol. Soc. Am. Bull., 85, 533-548, 1974.
Johnson, T., and P. Molnar, Focal mechanisms and plate tectonics of the southwest Pacific, J. Geophys. Res., 77, 5000-5032, 1972.
Langston, C. A., The effect of planar dipping structure on source and receiver responses for constant ray parameter, Bull. Seismol. Soc. Am., 67, 1029-1050, 1977.
Langston, C. A., and D. V. Helmberger, A procedure for modeling shallow dislocation sources, Geophys. J. R. Astron. Soc., 42, 117-130, 1975.
Letz, H., Seismizität in Irian Jaya (West-Neuguinea), Indonesien, und ihre tektonische Bedeutung (in German), Berl. Geowiss. Abh. Reihe A, B/12, 1985.
Lowell, J. D., Spitsbergen Tertiary orogenic belt and the Spitsbergen fracture zone, Geol. Soc. Am. Bull., 83, 3091-3102, 1972.
McCaffrey, R., Active tectonics of the eastern Sunda and Banda arcs, J. Geophys. Res., in press, 1988.
McCaffrey, R., and G. A. Abers, SYN3: A program for inversion of teleseismic body waveforms on microcomputers, AFGL Tech. Rep., TR-88-0099, Air Force Geophys. Lab., Bedford, Mass., 1988.
McCaffrey, R., and J. Nábělek, The geometry of backarc thrusting along the eastern Sunda arc, Indonesia: Constraints from earthquake and gravity data, J. Geophys. Res., 89, 6171-6179, 1984.
McCaffrey, R., and J. Nábělek, Earthquakes, gravity and the origin of the Bali Basin: An example of a nascent continental fold-and-thrust belt, J. Geophys. Res., 92, 441-460, 1987.
Minster, J. B., and T. H. Jordan, Present-day plate motions, J. Geophys. Res., 83, 5331-5354, 1978.
Nábělek, J., Determination of earthquake source parameters from inversion of body waves, Ph.D. thesis, 262 pp., Mass. Inst. of Technol., Cambridge, 1984.
Nábělek, J., Geometry and mechanism of faulting of the 1980 El Asnam, Algeria, earthquake from inversion of teleseismic body waves and comparison with field observations, J. Geophys. Res., 90, 12,713-12,728, 1985.
Nelson, M. R., R. McCaffrey, and P. Molnar, Source parameters for 11 earthquakes in the Tien Shan, Central Asia, determined by P and SH waveform inversion, J. Geophys. Res., 92, 12,629-12,648, 1987.
Pigram, C. J., and H. L. Davies, Terranes and the accretion history of the New Guinea orogen, BMR J. Aust. Geol. Geophys., 10, 193-211, 1987.

Pigram, C. J., and H. Panggabean, Geological data record, Wagheet (Yapekopra) 1:250,000 sheet area, Irian Jaya, Geol. Resour. Dev. Centre, Bandung, Indonesia, 1983.

Ripper, I. D., and K. F. McCue, The seismic zone of the Papuan fold belt, BMR J. Aust. Geol. Geophys., 8, 147-156, 1983.

Silver, E. A., and R. B. Smith, Comparison of terrane accretion in Southeast Asia and the Mesozoic North American Cordillera, Geology, 11, 198-202, 1983.

Smithson, S. B., J. A. Brewer, S. Kaufman, J. E. Oliver, and C. A. Hurich, Structure of the Laramide Wind River uplift, Wyoming, from COCORP deep reflection data and from gravity data, J. Geophys. Res., 84, 5955-5972, 1979.

Suárez, G., P. Molnar and B. C. Burchfiel, Seismicity, fault plane solutions, depth of faulting, and active tectonics of the Andes of Peru, Ecuador, and southern Colombia, J. Geophys. Res., 88, 10,403-10,428, 1983.

Taylor, B., Bismarck Sea: Evolution of a back-arc basin, Geology, 7, 171-174, 1979.

Visser, W. A. and J. J. Hermes, Geological results of the exploration for oil in the Netherlands New Guinea, Verh. K. Ned. Geol. Mijnbouwkd. Genoot., 20, 1-265, 1962.

Weissel, J. K., B. Taylor, and G. D. Karner, The opening of the Woodlark Basin, subduction of the Woodlark spreading system, and the evolution of northern Melanesia since mid-Pliocene time, Tectonophysics, 87, 253-277, 1982.

Wiens, D. A., Effects of near source bathymetry on teleseismic P waveforms, Geophys. Res. Lett., 14, 761-764, 1987.

G. Abers, 54-724, Department of Earth, Atmospheric, and Planetary Sciences, Massachusetts Institute of Technology, Cambridge, MA 02139.

R. McCaffrey, Department of Geology, Rensselaer Polytechnic Institute, Troy, NY 12181.

(Received December 16, 1987;
revised May 31, 1988;
accepted April 8, 1988.)